Inelastic scattering of slow electrons from Si(111) surfaces

B. N. J. Persson
Institut für Festkörperforschung der Kernforschungsanlage Jülich, Postfach 1913, D-5170 Jülich, West Germany

J. E. Demuth
IBM Thomas J. Watson Research Center, Yorktown Heights, New York 10598

(Received 14 March 1984)

Inelastic-electron-scattering measurements from Si(111)-7×7 and thin metal films on Si(111) are obtained for several different temperatures and analyzed with use of dipole scattering theory. A detailed discussion of the shape and temperature dependence of the quasielastic peak is presented. In particular, we show how the temperature-dependent width of the quasielastic peak can be used to obtain information regarding the surface free-carrier density, surface effective mass, and the surface conductivity. Analysis of the Si(111)-7×7 surface suggests an unusual surface electronic structure where a narrow state occurs within a surface-state band gap and determines the Fermi-level position. Analysis of Au and Pd metal films on Si(111) allows us to determine film resistivities as well as delineate microstructural features which influence surface transport properties.

I. INTRODUCTION

In recent years, electron-energy-loss spectroscopy (EELS) has emerged as an important experimental method to study surfaces. In these experiments a beam of almost monoenergetic electrons are incident upon a surface. By analyzing the energy distribution of the scattered electrons, information about the electronic and vibrational properties of the surface can be obtained.

An important aspect of EELS is that most of the experimental data can be analyzed using the relative simple dipole scattering theory which accounts for the long-range Coulomb interaction between the incident electrons and the medium.[1] Here, the excitation process starts when the electrons are at a large distance d from the surface, where $d \sim (2E_0/\hbar\omega)/k_0$, with $E_0 = \hbar^2 k_0^2/2m$ being the kinetic energy of the incident electron and $\hbar\omega$ the energy transfer to the excitation in the medium. The momentum transfer is therefore small, $q_{\parallel} \sim 1/d \sim k_0 \hbar\omega/2E_0$, and the dipole-scattered electrons form a narrow lobe centered close to the specular direction. The width of the lobe is $\Delta\theta \sim \hbar\omega/2E_0$.

In this work we will mainly focus on the inelastic scattering which involves very small loss energies, typically $\hbar\omega$ equal to a few milli-electron-volts. For an incident electron with energy $E_0 \approx 10$ eV one finds $d \approx 10^4$ Å and $\Delta\theta \approx 0.01°$. Thus, these very-low-energy excitations start when the electron is very far away from the surface and the inelastically scattered electrons form an extremely narrow lobe located almost in the specular direction. As a consequence of the latter fact, all the scattered electrons pass into the acceptance angle of the analyzer (typically $\sim 1°$). Note also that since the excitation process starts far away from the surface, it is possible to use the simplest version of the dipole scattering theory, which neglects the electron-image electron force. Additionally, since the energy and momentum transfer to the excitations in the medium is so small, the reflectivity of the elastically and inelastically scattered electrons will be practically identical. All these facts together make the dipole scattering theory a highly accurate theory in the study of the quasielastic peak and very-low-energy excitation processes.

Dipole scattering theory, in its simplest form, is a single-scattering theory where the incident electron is assumed to scatter inelastically from the surface at most once. This theory is valid for most practical purposes, e.g., in studies of vibrations in adsorbates or interband transitions in the substrate. As pointed out earlier, for small loss energies $\hbar\omega$, the distance d from the surface where the excitation process starts will be very large. As a result, for sufficiently small $\hbar\omega$ one must, in general, account for multiple losses. At which loss energy multiple scattering starts to be important depends strongly on the particular physical system under consideration and also on the temperature. For example, for a thin metal overlayer on top of silicon and at room temperature, inelastic multiple scattering occurs when $\hbar\omega \lesssim 35$ meV. Since the instrumental resolution of a typical EEL spectrometer is about 10 meV, the multiple scattering will appear mainly as a broadening of the "elastic peak." The study of the shape and temperature dependence of this quasielastic peak for several important physical systems is the main aim of the present work. Our work is the first to quantitatively consider and analyze these multiple-scattering processes. The theoretical results will be illustrated with two applications, the 7×7 reconstructed Si(111) surface and thin Au and Pd films on Si(111).

The 7×7 reconstructed Si(111) surface is one of the most studied systems in surface science.[2] Despite this, very little is known about its electronic structure[3] and about the driving force for the reconstruction.[4] We will present and analyze inelastic-electron-scattering data from Si(111)-7×7 obtained for several different temperatures, which suggests that this surface has an unusual electronic structure. In earlier work by Backes and Ibach,[5] the same

system was studied at room temperature and without analyzing the width of the quasielastic peak. Our analysis of these latter features provides a physically different picture of Si(111)-7×7 than achieved in this earlier work[5] or other studies.

The structure of thin metal overlayers on top of semiconductors has been studied with EELS by Backes and Ibach[6] and by Dubois *et al.*[7] However, these authors again analyzed only the loss data in the single-scattering regime, while we focus on the multiple-scattering regime. We will derive a very simple formula for the width of the quasielastic peak which agrees well with the experimental data, and from which the conductivity properties of the metal films can be deduced almost trivially.

This work is divided as follows. In Secs. II and III we review some basic equations which relate to inelastic electron scattering from surfaces. Section IV contains a short introductory discussion of what is known about the electronic structure of the Si(111)-7×7 surface from photoemission measurements. In Sec. V we present experimental EELS data and in Secs. VI and VII these data are analyzed theoretically. Section VIII contains a discussion of the experimental and theoretical results. In Sec. IX we present a detailed discussion of the shape and temperature dependence of the quasielastic peak in a general case, and in Sec. X we present illustrative applications to thin metal films on Si(111). Section XI contains a summary. Appendixes A—E contain the derivations of the main theoretical results and form an important part of this work.

II. INELASTIC ELECTRON SCATTERING FROM SURFACES

The experimental results to be presented in Sec. V are obtained by electron-energy-loss spectroscopy. Here we will briefly review some of the basic equations which relate to EELS.

Let us first define the surface response function $g(q_{||},\omega)$ which plays an important role in what follows. Consider a semi-infinite medium (Si in our case) occupying the half space $z>0$. Let

$$\phi_{\text{ext}}(\vec{x},t)=e^{i\vec{q}_{||}\cdot\vec{x}_{||}-q_{||}z-i\omega t} \tag{1}$$

be an external potential which polarizes the medium. The induced polarization changes will give rise to an induced potential which for $z<0$ (i.e., outside the medium) can be written as

$$\phi_{\text{ind}}(\vec{x},t)=-g(q_{||},\omega)e^{i\vec{q}_{||}\cdot\vec{x}_{||}+q_{||}z-i\omega t} . \tag{2}$$

This equation defines $g(q_{||},\omega)$. It is implicitly assumed that the media can be treated as translationally invariant parallel to the surface.

Now consider an electron with a few electron volts energy incident upon the surface. The electric field from the electron penetrates into the media where it can excite, e.g., electron-hole pairs, plasmons, or phonons. Let $\vec{k}$ and $\vec{k}'$ denote the wave vectors of an incident and inelastically scattered electron, respectively. Thus $\hbar\vec{q}_{||}=\hbar(\vec{k}_{||}-\vec{k}'_{||})$ is the momentum transfer (parallel to the surface) to the excitation in the media and $\hbar\omega=\hbar^2(k^2-k'^2)/2m$ is the energy transfer. Let $P(\vec{k},\vec{k}')d\Omega_{k'}d(\hbar\omega)$ be the probability that an incident electron is scattered inelastically into the range of energy losses between $\hbar\omega$ and $\hbar(\omega+d\omega)$, and into the solid angle $d\Omega_{k'}$ around the direction of $\vec{k}'$. For small momentum transfer, $q_{||}\ll k$, and for "weak" scattering (to be defined below), one has, from standard dipole scattering theory,[1]

$$P(\vec{k},\vec{k}')=\frac{2}{(ea_0\pi)^2}\frac{1}{\cos\alpha}\frac{k'}{k}\frac{q_{||}}{|q_{||}^2+q_{\perp}^2|^2}\,\text{Img}(q_{||},\omega)$$

$$\equiv A(\vec{k},\vec{k}')\,\text{Img}(q_{||},\omega) , \tag{3}$$

where $q_{\perp}=k_z-k'_z$, and α is the angle of incidence. Thus the inelastic scattering probability is a product of two factors—a kinematic factor $A(\vec{k},\vec{k}')$ which depends strongly on the loss energy $\hbar\omega$ ($A\sim\omega^{-3}$ as $\omega\to 0$), but which is independent of the properties of the medium, and the loss function $\text{Img}(q_{||},\omega)$ which is proportional to the power absorption in the medium due to an external potential of the form (1). $g(q_{||},\omega)$ enters the inelastic scattering probability (3) because it determines the induced electric field outside the substrate [via (2)] and it is this time-varying field that can scatter the incident electron inelastically. We note that Eq. (3) is valid at zero temperature—at a finite temperature there is an extra factor $(n_\omega+1)$ where

$$n_\omega=[\exp(\hbar\omega/k_BT)-1]^{-1}$$

is the Bose-Einstein factor.

Equation (3) is based on a single-scattering theory, i.e., the incident electron is assumed to scatter inelastically at most once. However, if the coupling to the medium is strong or if the loss energies are very small, so that the interaction occurs during a very long time (see the Introduction), then an incident electron can undergo multiple inelastic scattering. At small loss energies the full lobe of inelastically scattered electrons passes into the analyzer and the measured relative loss intensity (in the single-scattering regime) is therefore proportional to

$$P_s(\omega)=\int d\Omega_{\vec{k}'}P(\vec{k},\vec{k}') , \tag{4}$$

where the integral can be taken over the whole solid angle 4π. The index s on P_s stands for single scattering. To obtain the probability for multiple scattering one can proceed as follows: Assume that the excitations in the substrate can be treated as independent bosons. Let $\hbar\omega_{\vec{q}}$ be the energy of the excitation with wave vector $\vec{q}$. Consider now the independent boson Hamiltonian,

$$H=\sum_{\vec{q}}\hbar\omega_{\vec{q}}b^{\dagger}_{\vec{q}}b_{\vec{q}}+F(t)\sum_{\vec{q}}M_{\vec{q}}(b^{\dagger}_{\vec{q}}+b_{\vec{q}}) .$$

Here, $F(t)$ is the time-dependent force exerted on the oscillators by an incident electron, which is treated as a classical point particle moving along a well-defined trajectory. The probability, at zero temperature, for excitation of an oscillator from its ground state to a final state n_q, is

$$P(0\to n_{\vec{q}})=\frac{1}{(n_{\vec{q}})!}(B_{\vec{q}})^{n_{\vec{q}}}e^{-B_{\vec{q}}}, \tag{5}$$

where

$$B_{\vec{q}}=\left|\frac{(M_{\vec{q}})^{1/2}}{\hbar}\int_{-\infty}^{\infty}dt\,F(t)e^{i\omega_{\vec{q}}t}\right|^2 .$$

Since the bosons are independent, it is now trivial to calculate the probability $P(\omega)$ (at zero temperature) that the incident electron loses energy $\hbar\omega$:

$$P(\omega)=\sum_{n_{\vec{q}_1}=0}\sum_{n_{\vec{q}_2}=0}\cdots P(0\to n_{\vec{q}_1})P(0\to n_{\vec{q}_2})\times\cdots \times\delta(\omega-n_{\vec{q}_1}\omega_{\vec{q}_1}-n_{\vec{q}_2}\omega_{\vec{q}_2}-\cdots), \tag{6}$$

where $\vec{q}_1,\vec{q}_2,\ldots$ denotes the different $\vec{q}_{||}$. Now since

$$\delta(\omega-n_{\vec{q}_1}\omega_{\vec{q}_1}-\cdots)=\frac{1}{2\pi}\int dt\,e^{-i(\omega-n_{\vec{q}_1}\omega_{\vec{q}_1}-\cdots)t}, \tag{7}$$

we obtain from (5)—(7),

$$P(\omega)=\frac{1}{2\pi}\int dt\,e^{-i\omega t}\exp\left[\sum_{\vec{q}}B_{\vec{q}}(e^{i\omega_{\vec{q}}t}-1)\right]. \tag{8}$$

In the weak-coupling limit (i.e., $B_{\vec{q}}\to 0$), we obtain

$$\exp\left[\sum_{\vec{q}}B_{\vec{q}}(e^{i\omega_{\vec{q}}t}-1)\right]\approx 1+\sum_{\vec{q}}B_{\vec{q}}(e^{i\omega_{\vec{q}}t}-1),$$

and thus

$$P(\omega)\approx\left[1-\sum_{\vec{q}}B_{\vec{q}}\right]\delta(\omega)+\sum_{\vec{q}}B_{\vec{q}}\delta(\omega-\omega_{\vec{q}}).$$

The second term in $P(\omega)$ describes single scattering, so that at zero temperature,

$$P_s(\omega)=\sum_{\vec{q}}B_{\vec{q}}\delta(\omega-\omega_{\vec{q}}).$$

We now multiply this equation with $e^{i\omega t}-1$ and integrate over ω to obtain

$$\int_0^{\infty}d\omega\,P_s(\omega)(e^{i\omega t}-1)=\sum_{\vec{q}}B_{\vec{q}}(e^{i\omega_{\vec{q}}t}-1).$$

Substituting this expression into (8) gives

$$P(\omega)=\frac{1}{2\pi}\int dt\,e^{-i\omega t}\exp\left[\int_0^{\infty}d\omega' P_s(\omega')(e^{i\omega' t}-1)\right].$$

This formula gives the inelastic scattering probability at zero temperature. The finite-temperature generalization of this expression has been derived by Lucas and Šunjić[8] and Schaich:[9]

$$P(\omega)=\frac{1}{2\pi}\int dt\,e^{-i\omega t}\times\exp\left[\int_0^{\infty}d\omega' P_s(\omega')[(n_{\omega'}+1)(e^{i\omega' t}-1)+n_{\omega'}(e^{-i\omega' t}-1)]\right], \tag{9}$$

where

$$n_{\omega}=[\exp(\hbar\omega/k_BT)-1]^{-1}$$

is the Bose-Einstein factor. We will use (9) in Sec. VII, where we calculate the line shape of the quasielastic peak for electrons inelastically scattered from the Si(111)-7×7 surface.

III. STRUCTURE OF $g(q_{||},\omega)$

We will assume that the 7×7 reconstructed Si(111) surface can be treated as a two-dimensional electronic system on top of a semi-infinite dielectric medium characterized by the bulk dielectric constant $\epsilon(\omega)$, which for small loss energies can be treated as a constant, $\epsilon\approx 11.7$. Within this model it is almost trivial to derive an expression for $g(q_{||},\omega)$. Consider the response of the system to an external potential of the form given by Eq. (1). The electric potential outside the medium ($z<0$) will then be

$$\phi_<=(e^{-q_{||}z}-g\,e^{q_{||}z})e^{i(\vec{q}_{||}\cdot\vec{x}_{||}-\omega t)}.$$

The electric potential in the medium satisfies $\nabla^2\phi=0$, and can therefore be written as

$$\phi_>=t\,e^{-q_{||}z}e^{i(\vec{q}_{||}\cdot\vec{x}_{||}-\omega t)}.$$

It is convenient to imagine there is an infinitesimal separation between the two-dimensional electronic system and the underlying medium; see Fig. 1. In the vacuum region in between the system and the underlying medium, the potential takes the form

$$\phi_0=(a\,e^{q_{||}z}+b\,e^{-q_{||}z})e^{i(\vec{q}_{||}\cdot\vec{x}_{||}-\omega t)}.$$

Both the potential ϕ and $\epsilon\,d\phi/dz$ must be continuous at the vacuum-medium interface, which gives

$$t=a+b,\quad -\epsilon t=a-b,$$

from which one obtains

$$\epsilon(a+b)+(a-b)=0. \tag{10}$$

Next, the discontinuity of the electric field over the two-dimensional electronic system must be related to the sur-

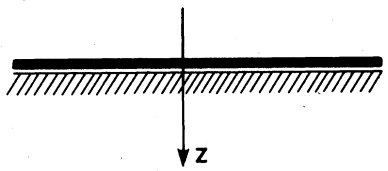

FIG. 1. Semi-infinite medium with a two-dimensional electronic system on top.

face charge density $\sigma(q_{||},\omega)$ in the two-dimensional electronic system in the usual way

$$\left.\frac{d\phi}{dz}\right|_{+} - \left.\frac{d\phi}{dz}\right|_{-} = -4\pi\sigma ,$$

or

$$(a-b)-(-1-g) = -4\pi\sigma/q_{||} . \tag{11}$$

Furthermore, the electric potential itself must be continuous across the two-dimensional electronic system, which gives

$$a+b = 1-g . \tag{12}$$

From Eqs. (10)—(12) we obtain

$$g = \frac{\epsilon-1}{\epsilon+1} - \frac{4\pi}{\epsilon+1}\frac{\sigma}{q_{||}} .$$

If we define the surface polarizability $\chi(q_{||},\omega)$ by

$$\sigma(q_{||},\omega) = \chi(q_{||},\omega)\phi(q_{||},\omega) ,$$

where $\phi(q_{||},\omega)$ is the potential in the two-dimensional system, i.e., $\phi = 1-g$; then we obtain

$$g = \frac{\epsilon-1}{\epsilon+1} - \frac{4\pi}{1+\epsilon}\frac{\chi}{q_{||}}(1-g) ,$$

or

$$g = 1 - \frac{2}{\epsilon+1-4\pi\chi/q_{||}} .$$

Thus

$$\mathrm{Im}g(q_{||},\omega) = -\mathrm{Im}\frac{2}{\epsilon+1-4\pi\chi(q_{||},\omega)/q_{||}} . \tag{13}$$

Mills[10] has derived an expression for Img for a thin dielectric film (thickness d) with a dielectric function $\epsilon_1(\omega)$ on top of a semi-infinite dielectric with a dielectric function $\epsilon(\omega)$. For $q_{||}d \ll 1$, Mills[10] obtained

$$\mathrm{Im}g = -\mathrm{Im}\frac{2}{\epsilon+1+q_{||}d[\epsilon_1(\omega)-\epsilon^2/\epsilon_1(\omega)]} . \tag{14}$$

This result differs from (13) in two ways: First, (13) accounts (if necessary) for spatial nonlocality within the two-dimensional system via the dependence of $\chi(q_{||},\omega)$ on $q_{||}$. Second, the term $\epsilon^2/\epsilon_1(\omega)$ within the parentheses in (14) has no analog in (13). However, this term disappears from (14) in the limit $d\to 0$ and $\epsilon_1\to\infty$, with $d\epsilon_1 = \text{const}$.

Suppose that it is possible to use an independent-particle picture to describe the electronic structure of the Si(111)-7×7 surface. Then, contributions to $\chi(q_{||},\omega)$ will arise from interband and (if there is a partly filled band) intraband transitions. For small $q_{||}$, which is the case relevant to us, the contribution from interband transitions can be written as

$$\chi_{\text{interband}} \approx -q_{||}^2 n_0 \alpha(\omega) , \tag{15}$$

where $n_0\alpha(\omega)$ is the polarizability per unit area (n_0 is the number of Si atoms per unit area). The contribution from intraband transitions can, for $q_{||}a \ll 1$ (where a is the surface lattice constant), be written as

$$\chi_{\text{intraband}} \approx 2e^2 \int \frac{d^2k}{(2\pi)^2}\frac{f_k - f_{k+q}}{\hbar\omega - (\epsilon_{k+q}-\epsilon_k)} , \tag{16a}$$

where we assume that ϵ_k is well approximated by $\epsilon_k = \hbar^2k^2/2m^*$ and where f_k is the Fermi-Dirac distribution function. If $q_{||} \ll k_F$ and $(\omega/\omega_F)(k_F/q_{||}) \gg 1$, then one can expand (16a) to second order in $q_{||}$ to obtain

$$\chi_{\text{intraband}} \approx \frac{e^2 n}{m^*\omega^2} q_{||}^2 , \tag{16b}$$

where n is the number of free carriers per unit surface area. Substituting (15) and (16b) into (13) gives

$$\mathrm{Im}g = -\mathrm{Im}\frac{2}{\epsilon+1+4\pi n_0\alpha q_{||} - 4\pi n e^2 q_{||}/(m^*\omega^2)} . \tag{17}$$

IV. ELECTRONIC STRUCTURE OF Si(111)-7×7

As background for what will follow, this section reviews what is known from photoemission experiments[11] about the electronic structure of Si(111)-7×7. First consider the fictitious case of an unreconstructed Si(111) surface. This surface will have dangling bonds perpendicular to the surface arranged in a two-dimensional lattice structure. Extensive numerical calculations[12] have shown that these dangling bonds form a surface-electron band which occurs in the gap between the bulk valence and conduction bands of Si, as schematically shown in Fig. 2(a). (This result is expected from simple physical arguments; see Harrison, Ref. 13.) A dangling-bond state containing one unpaired electron is an energetically unstable configuration which tries to lower its energy by pairing up with another unpaired dangling bond, forming a double occupied bonding orbital and an unoccupied antibonding orbital. In the absence of adsorbed gases this requires the Si atoms change their positions, thereby giving rise to a reconstruction. When a Si(111) surface is generated by cleaving in vacuum and at room temperature, it will reconstruct into a 2×1 structure. This is, however, not the ground state, and when the Si(111) surface is heated to

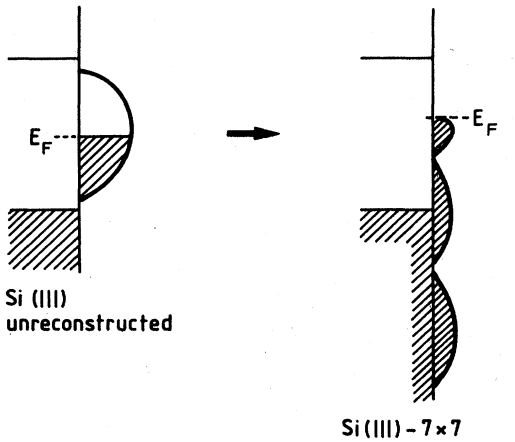

FIG. 2. Schematic representation of the surface density of states of an unreconstructed surface (left) and for a 7×7 reconstructed surface (right).

$\simeq$600 °C, it reconstructs into the much more complicated 7×7 structure. Figure 2(b) shows the surface density of states for the 7×7 reconstructed surface as deduced from photoemission experiments. The "center of mass" of the surface density of states is obviously displaced towards lower energies, compared with the unreconstructed surface which indicates that the 7×7 surface is more stable.

Since there is an odd number of electrons in the 7×7 unit cell, if an independent-particle picture is valid, then there must be at least one partly filled band of surface states making the Si(111) surface metallic. This is consistent with the photoemission data, which show a surface density-of-states peak in the vicinity of the Fermi energy E_F. However, the resolution of photoemission experiments ($\sim$0.1 eV) is not sufficient to resolve the detailed surface-state structure near E_F and tell whether there is a finite density of states at E_F. It will be shown in the following sections that EELS can provide us with an answer to this question.

V. EXPERIMENTAL PROCEDURE

These measurements were performed in an ion-turbomolecular-titanium sublimator-pumped ultrahigh-vacuum system having a base pressure of 4×10^{-11} Torr. This system contains a cylindrical mirror analyzer (CMA) for Auger and ultraviolet photoemission spectroscopy (UPS), a three-grid Varian Associates low-energy electron-diffraction (LEED) optics, and a set of hemispherical deflection analyzers (2.5 cm diam) for high-resolution electron-energy-loss measurements (EELS). A boron-doped sample (1.3×10^{15} atoms/cm^2) was ultrasonically machined to size (9 mm diam and 1.5 mm thick), mechanically and chemically polished, and physically clamped to the sample support by a tantalum retaining ring. The sample could be indirectly cooled and heated between 15 and 1400 K, as measured with a Chromel-Alumel thermocouple spot-welded to the retaining ring and/or an infrared pyrometer. Cooling of the sample was preceded by cooling of the cryostat which reduced system pressures below 2×10^{-11} Torr and virtually eliminated ambient contamination during cool down and measurements at low temperatures. The sample was cleaned by initial argon-ion bombardment (400 V) followed by *repeated* oxidation cycles, annealing to 1350 K, and slow cooling to produce atomically clean, well-ordered, 7×7 surfaces.

Palladium was evaporated by resistively heating a Pd wire, while Au was evaporated from a Au bead on a W filament. In both cases, system pressures remained in the 10^{-10}-Torr range during evaporation, and EELS and UPS did not detect any co-absorbed background impurities. After metal evaporations it was not possible to achieve the same initial 7×7 surface due to a small concentration of palladium impurities ($\sim$1 at.%), which could not be removed. These impurities eliminated the surface states seen in UPS right near E_F, prevented any detectable (temperature-dependent) elastic beam broadening from occurring, and produced a 1×1 LEED pattern. One advantage of these impurities is that they thus provide no elastic beam broadening from the starting surface, so as to allow us to analyze the beam broadening arising after metal evaporation.

EELS was performed using a fixed total scattering angle of 90°, and for specular scattering conditions ($\alpha=45°$) and incident-beam energies (12—20 eV) where optical (dipole) selection rules are applicable. The beam energy was calibrated by the zero-kinetic-energy "cutoff" of the loss spectrum. Off-specular measurements confirm that the features we report here are dipole excited. Our EELS resolution, as determined after reflection from the crystal, was typically 7—9 meV [full width at half maximum (FWHM)], but was degraded to 20 meV to examine the lower-intensity losses above 0.5 eV. Measurements of the temperature-dependent beam broadening were performed (with the ion gauge off) on both clean and metallized surfaces by initial cooling to 20 K followed by continuous monitoring of the elastic beam and temperature after terminating the He flow. Temperature cycling back to 20 K, as well as nitrogen cooling to 78 K directly, were used to check for possible contamination effects during warm up.

Figure 3 shows the loss spectra at room temperature ($T=228$ K) and $T=20$ K obtained for an incident kinetic energy $E_0=12$ eV and a total acceptance angle $\theta_1=2°$. Several different acceptance angles from 0.75—2° were utilized with comparable results: The 2° acceptance angle provided the best signal-to-noise ratio in the loss region, and was therefore used to determine Img in Fig. 4. The room-temperature data are quite structureless and monotonically decreasing out to $\hbar\omega\approx1$ eV. The low-temperature data have more structure, particularly for small loss energies, $\hbar\omega\sim50$ meV. Note also that the width of the quasielastic peak depends strongly on temperature: it increases from about 8.8 meV at $T=15$ K to 13 meV at $T=288$ K. We will discuss this in greater detail in Sec. VII, but we point out already here that it is caused by multiple excitations of very-low-energy plasmons in the

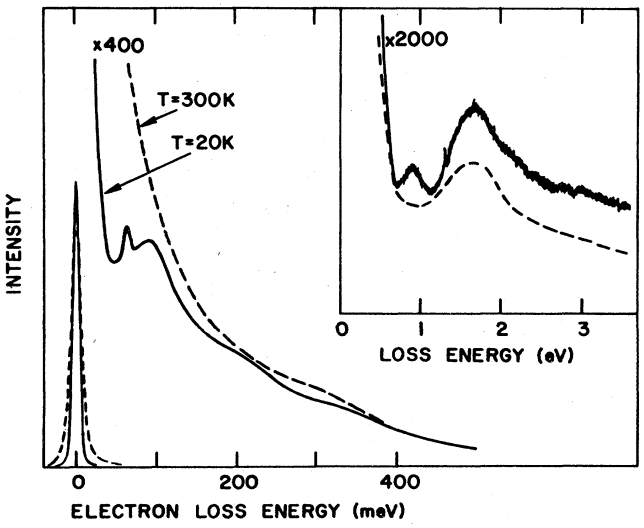

FIG. 3. Electron-energy-loss data from Si(111)-7×7 for two temperatures, $T=300$ and 20 K. Incident-electron energy $E_0=15$ eV, angle of incidence $\alpha=45°$, and half-angle of analyzer $\theta_1=2°$.

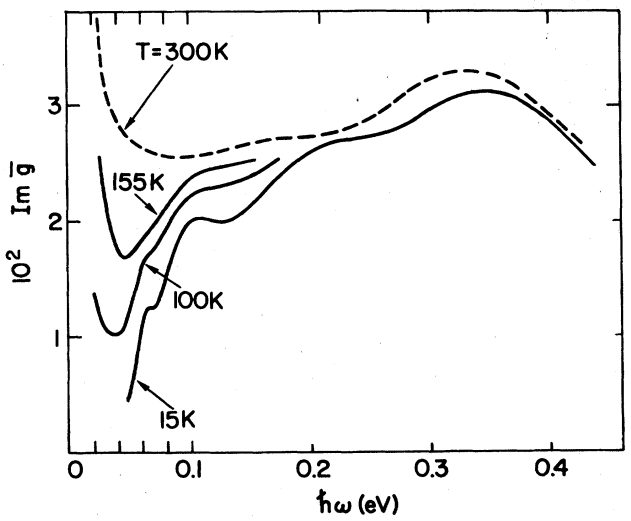

FIG. 4. Surface loss function Im$\bar{g}$ for Si(111)-7×7 as a function of the loss energy $\hbar\omega$ for four different temperatures, $T=300$, 155, and 100, and 15 K. $E_0=12$ eV, $\alpha=45°$, and $\theta_1=2°$.

surface. The inset of Fig. 3 shows two loss peaks at about $\hbar\omega\approx 0.9$ and 1.7 eV. These features are sensitive to absorption and are likely surface interband transitions (the 1.7-eV peak also having a contribution from bulk interband transitions), but they will not be discussed in the following. In the next section we will analyze the structure between $35\leq\hbar\omega\leq 400$ meV where the single-scattering dipole scattering theory is applicable. For $\hbar\omega\lesssim 35$ meV, multiple scattering becomes important: This loss region will be analyzed in Sec. VII using the multiple-scattering formula (9).

VI. ANALYSIS OF EXPERIMENTAL DATA IN THE SINGLE-SCATTERING REGION

For $\hbar\omega\geq 35$ meV, inelastic multiple scattering is negligible (see Sec. IX), and the experimental data for these loss energies can therefore by analyzed using the single-scattering formula (3). In EELS one does not measure $P(\vec{k},\vec{k}')$ directly, but rather $P(\vec{k},\vec{k}')$ integrated over the solid angle of detection $\Delta\Omega$; we write

$$\Delta P(\omega)=\int_{\Delta\Omega} d\Omega_{k'} P(\vec{k},\vec{k}') .$$

In Fig. 4 we show Im$\bar{g}(\omega)$ defined by

$$\mathrm{Im}\bar{g}(\omega)=\frac{\int_{\Delta\Omega} d\Omega_{k'} A(\vec{k},\vec{k}')\,\mathrm{Im}g(q_{||},\omega)}{\int_{\Delta\Omega} d\Omega_{k'} A(\vec{k},\vec{k}')} . \tag{18}$$

Thus Im$\bar{g}$ is obtained by dividing the experimental loss spectrum in Fig. 3 by the kinematic dipole scattering factor $A(\vec{k},\vec{k}')$ integrated over the solid angle of detection. If Img is independent or only weakly dependent on $q_{||}$, then Im$\bar{g}$=Img. In any case, dividing out the strong-ω-dependent factor $A(\vec{k},\vec{k}')$, according to (18), gives a quantity which is largely an intrinsic property of the substrate and thus much easier to interpret physically than the original loss spectrum $\Delta P(\omega)$.

Figure 4 shows Im$\bar{g}(\omega)$. Note that as the temperature is lowered, a band gap of about 40 meV tends to open up. The low-temperature curves are rather uncertain for $\hbar\omega\leq 35$ meV because they involve subtracting away the tail of the elastic beam from the data in Fig. 3. This tail was obtained from a hydrogen-saturated Si(111) surface where the entire loss background up to $\hbar\omega\sim 1$ eV has disappeared. At room temperature the gap seems to have disappeared. However, the broadening of the quasielastic peak caused by multiple excitations of low-energy plasmons produces "wings" which could obscure this gap as well as its temperature dependence. Thus, it is not clear to what extent the temperature dependence of this gap arises from electron-phonon effects, as is suggested for the higher-lying transitions.

Using a sum rule one can obtain the oscillator strength contained in the structure between $40<\hbar\omega<450$ meV. The result is 5 ± 1 electrons per 7×7 unit cell.

VII. ANALYSIS OF EXPERIMENTAL DATA IN THE MULTIPLE-SCATTERING REGION.

As pointed out in the preceding section, within a one-particle picture there must be at least one partly filled band at the Fermi energy. The last term in the denominator of (17) accounts for this partly filled band. For sufficiently small ω, Eq. (17) takes the form

$$\mathrm{Im}g=-\mathrm{Im}\frac{2}{\epsilon+1-4\pi ne^2 q_{||}/(m^*\omega^2)}$$
$$=\frac{2\pi}{(\epsilon+1)^2}\frac{4\pi ne^2}{m^*}q_{||}\delta(\omega^2-4\pi ne^2 q_{||}/[m^*(1+\epsilon)]) . \tag{19}$$

Here we have neglected the screening by the interband-transition term $4\pi n_0\alpha q_{||}$ since this is a very good approximation for those ω and $q_{||}$ which are relevant here. Substituting (19) in (3) and integrating $P(\vec{k},\vec{k}')$ over the solid angle of the entire upper half plane gives (see Appendix A)

$$P_s(\omega)=\int d\Omega_{k'} P(\vec{k},\vec{k}')=\frac{C}{\hbar\omega} f(\omega/\beta,\alpha) , \tag{20}$$

where

$$C=\frac{4}{\pi}\frac{1}{\epsilon+1}\frac{1}{\cos^2\alpha}\frac{1}{ka_0} , \tag{21}$$

and

$$f(x,\alpha)=\frac{1}{x}\int_0^{2\pi} d\phi\left[1+\left[\frac{1/x}{\cos\alpha}-\tan\alpha\cos\phi\right]^2\right]^{-2} \tag{22}$$

and

$$\beta=\frac{4\pi ne^2}{m^*(\epsilon+1)}\frac{1}{v} ,$$

where v is the velocity of the incident electron. Note that

$x=\omega/\beta$, and C, are dimensionless. The integral (22) can be evaluated analytically, but the result is complicated: It is easier to calculate f directly from (22) by numerical integration, or by use of the following simple, but accurate, formula:

$$f \approx \frac{1.57x^3}{1+0.47x^4-0.4x}, \quad \alpha=45^\circ .$$

This expression has the correct limiting forms ($\alpha=45°$):

$$f \to \frac{\pi}{x}(1+\cos^2\alpha)\cos\alpha \approx \frac{1.57}{0.47}\frac{1}{x} \quad \text{as } x \to \infty ,$$

$$f \to 2\pi x^3 \cos^4\alpha \approx 1.57x^3 \quad \text{as } x \to 0 .$$

Substituting $P_s(\omega)$, as given by (20), into (9), and evaluating the integrals numerically gives the quasielastic peak. The result depends only on the parameter β, which has been chosen to give the best agreement between theory and experiment. The dashed lines in Fig. 5 show $P(\omega)$ for three different temperatures and with $\hbar\beta=0.2$ meV. Note that the temperature dependence of $P(\omega)$ is due to the Bose-Einstein factor n_ω. Since the incident electrons in EELS have a finite energy spread (typically 10 meV) around the mean energy E_0, one must broaden the dashed profiles in Fig. 5 according to the instrumental resolution in order to compare theory with experiment. By studying the elastic peak from a hydrogen-saturated Si(111) surface, we find a nearly-Gaussian-shaped peak with a FWHM of 8.4 meV. The solid curves in Fig. 5 show the theoretical result for the quasielastic peak after convoluting the dashed curves with a Gaussian with a FWHM of 8.4 meV. The circles are the experimental data which agree very well with the theoretical predictions. The small deviation between the theoretical curve and the experimental data points on the gain side is associated with focusing problem of the spectrometer in this particular run. The variation of the FWHM with temperature is shown in detail in Fig. 6. The agreement between theory and experiment is again very good (note that there is only one fitting parameter, β, in the theory). The dashed curve in Fig. 6 will be discussed in the next section.

Backes and Ibach[5] and Froitzheim *et al.*[14] have also performed EELS measurement on Si(111)-7×7. In Table I we have collected their results for the width of the quasielastic peak at room temperature, and also stated the experimental conditions under which these experiments were performed. Note, in particular, that their silicon samples have a much lower bulk doping than our sample ($n_A \sim 1.3\times10^{15}$ boron atoms/cm^3). Nevertheless, the theoretical predicted width for the quasielastic peak, using the value of n/m^* we find, also agrees with their experimental results. These results show that the observed broadening is reproducible and does not depend on the particular experimental conditions or bulk doping. This provides evidence that the broadening cannot be caused by the bulk doping (also see the next section) or by *random*, extrinsic imperfections at the surface which one might expect to vary between the different samples.

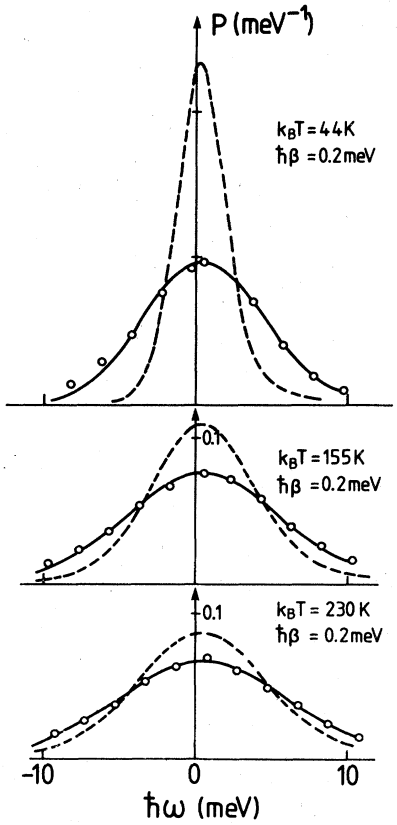

FIG. 5. Scattering probability $P(\hbar\omega)$ for three different temperatures, $T=230$, 155, and 44 K. The open circles denote the experimental data for $E_0=12$ eV and $\alpha=45°$. The dashed and solid lines represent the theoretically predicted results for $P(\hbar\omega)$ before and after convolution with a Gaussian with a FWHM of 8.4 meV. In the calculation, we used $\hbar\beta=0.2$ meV, $E_0=12$ eV, and $\alpha=45°$.

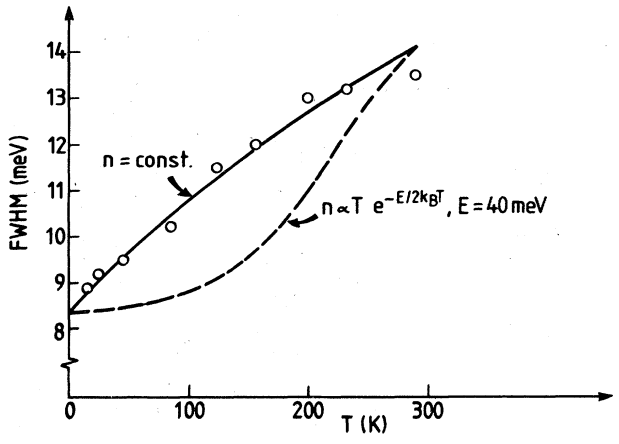

FIG. 6. Temperature dependence of the peak width (full width at half maximum) of the quasielastic peak from Si(111)-7×7. The open circles represent the experimental data and the solid line is the theoretical result with $\hbar\beta=0.2$ meV. The dashed line is the result of a theoretical model which assumes that three carriers are thermally excited so that $\hbar\beta \sim T\exp(-E_{\rm gap}/2k_BT)$, where $E_{\rm gap}=40$ meV is the band gap.

TABLE I. Results for the quasielastic peak width at room temperature.

α (deg)	E_0 (eV)	Γ_0 (meV)	Γ(expt) (meV)	Γ(theory) (meV)
	Backes *et al.*[a] ($n_A \approx 3.7\times10^{12}$ cm^{-3})			
65	7.3	11.7	18.9	19.7
	Froitzheim *et al.*[b] ($n_D \approx 10^{12}$ cm^{-3})			
60	5	6	19	18.8
	This work ($n_A \approx 1.3\times10^{15}$ cm^{-3})			
45	12	8.5	13.8	14

[a]Reference 5.
[b]Reference 14.

VIII. DISCUSSION

We saw in the preceding section that the temperature dependence of the FWHM of the quasielastic peak for electrons scattered from Si(111)-7×7 can be explained within a very simple model which attributes the broadening to multiple excitation of plasmons in a two-dimensional electronic system. Since there is an odd number of electrons in the 7×7 unit cell, in a independent-particle picture there must be at least one partly filled electronic band. The electrons in this band can perform low-frequency two-dimensional plasma oscillations.[15] Fitting the theory to the experimental data gave $\hbar\beta=0.2$ meV. Using the definition of β, which we now write,

$$\hbar\beta=\frac{m}{m^*}\frac{4\pi ne^2}{(\epsilon+1)k} ,$$

where k is the wave vector of the incident electron, we obtain $m^*\simeq 60m$ if $\hbar\beta=0.2$ meV and $n=1$ electron/[(7×7) unit cell]$\simeq 0.0016$ Å^{-2}. (For a discussion of m^*, see Appendix E.) With this effective mass one can estimate the bandwidth B:

$$B=2\frac{\hbar^2k_F^2}{2m^*}=2\pi\hbar^2n/m^*\simeq 1 \text{ meV} .$$

Thus the half-filled band is extremely narrow, and we are led to the picture of the electronic structure in the vicinity of the Fermi energy as shown in Fig. 7. To be consistent with the electron-energy-loss data in Fig. 4, there must be a band gap of about 40 meV between the partially occupied sharp band at E_F and the first unoccupied (occupied) density-of-states structure above (below) E_F. This model is consistent with a number of experimental observations.

(a) The broadening of the quasielastic peak disappears already with a very low concentration of absorbed hydrogen atoms. Based upon our relative exposures, LEED patterns and absolute coverage calibrations by Culbertson,[16] this occurs for $\theta\sim 0.01$ to 0.02, or about one H atom per 7×7 unit cell. This is expected since the band at the Fermi energy (which carries one electron per 7×7 unit cell) is the most easily polarizable electronic state on the Si(111)-7×7 surface, and therefore it is the first attacked by the hydrogen atoms.

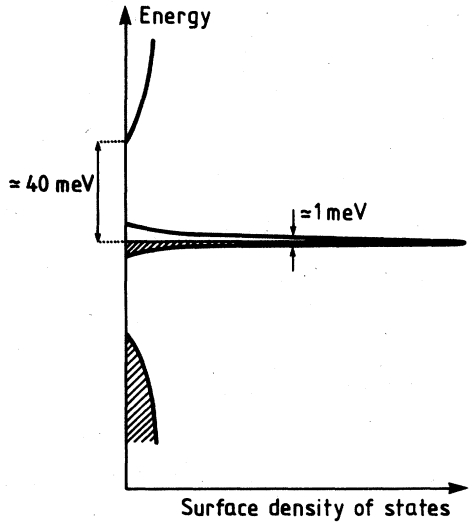

FIG. 7. If the Si(111)-7×7 has a half-filled electron band, then the theory predicts that it must be extremely narrow, about 1 meV wide.

(b) There seems to be *one* unique "active site" per 7×7 unit cell. That is, there is a site in the 7×7 unit cell which is much more reactive than others, as observed in absorption experiments involving hydrogen[17] and noble gases.[18] It is tempting to associate this single site with the large "holes" seen at the corners of the 7×7 unit cell in scanning-tunneling-microscope pictures.[19] We propose that these special sites are associated with the sharp band at the Fermi energy.

Thus the model we present seems to be consistent with all the *experimental* observations. However, there is one *theoretical* objection with this model associated with the narrow level. Since the bandwidth B is so small, the independent-particle picture on which the discussion has been based up to now must be questioned. For example, for a Hubbard Hamiltonian,

$$H=\sum_{i,\sigma}\epsilon_0\hat{n}_{i\sigma}+\sum_{i,j,\sigma}V_{ij}c_{i\sigma}^{\dagger}c_{j\sigma}+\sum_i U\hat{n}_{i\uparrow}\hat{n}_{i\downarrow} , \quad (23)$$

it is well known that if the bandwidth $B \ll U$ then the single-particle picture is incorrect and the ground will be spin polarized. The magnitude of U depends on how localized the state $c_{i\sigma}^{\dagger}|0\rangle$ is, but it is hard to imagine a case *where* $U<1$ *meV*. If $E(\vec{k})=\epsilon_0+V(\vec{k})$ denotes the eigenvalues of (23) when $U=0$, then the eigenvalues for $U\gg B$ are given by[20]

$$E^+(\vec{k})=\epsilon_0+U+V(\vec{k})/2,\quad E^-(\vec{k})=\epsilon_0+V(\vec{k})/2 .$$

Thus the electronic structure would in this case consist of a *filled* lower Hubbard band $E^-(\vec{k})$ and an *empty* upper Hubbard band $E^+(\vec{k})$. Such a system would not have any partly filled band, and would therefore not exhibit any low-frequency plasmons. We have therefore considered a number of alternative explanations which we will now discuss.

(a) Assume that there is a band gap of $\simeq$40 meV at the Fermi energy on Si(111)-7×7. At nonzero temperature

thermally excited electrons and holes will generate a low-density electron-hole plasma in which two-dimensional low-frequency plasma oscillations can occur just as discussed above. The broadening of the quasielastic peak will now depend on temperature not only via the Bose-Einstein factor but also because the number of thermally excited electrons and holes will depend (exponentially) on the temperature. That is, as the temperature is lowered the thermally excited electrons and holes will be "frozen out." The dashed line in Fig. 6 shows the theoretical result for the FWHM assuming that

$$n \sim T \exp[-E_{\rm gap}/(2k_B T)] ,$$

where $E_{\rm gap}=40$ meV is the band gap. Obviously, the agreement between theory and experiment is unsatisfactory and this process can therefore by ruled out.

(b) The incident electron will couple to the surface and bulk phonons of Si and this might give rise to the broadening of the quasielastic peak. However, as shown in Appendix B, coupling to phonons is, in general, too weak to explain the experimental results.

(c) If there is a non-negligible concentration of free carriers in the bulk and/or surface layers (say, due to unknown impurities), then these will exhibit a low-frequency plasma oscillation which can broaden the quasielastic peak. (This is also a reasonable possibility as our probe will "*sense*" $\sim 10^4$ *Å into the sample.*) It was suggested by Backes and Ibach[5] that this is not the case since hydrogen adsorption eliminates the broadening. However, this conclusion is not completely free from objections because adsorption of hydrogen changes the band bending and thus the concentration of free carriers at the Si(111) surface. However, the detailed discussion in Appendix C shows that the bulk free carriers cannot give rise to the observed broadening in the present case. This also follows from the observation made in Sec. VII, that the experimental data by Backes and Ibach[5] and by Froitzheim *et al.*[14] both show a broadening of the quasielastic peak which at room temperature agrees very well with our theoretical predictions. Since these n- and p-type samples had a bulk doping about 10^{-3} times smaller than our sample, one might anticipate widely different values of $\hbar\beta$ if bulk-derived, near-surface free carriers dominated the broadening.

Thus none of models (a)—(c) are consistent with all the experimental data. Thus, perhaps, the states $c_{i\sigma}^{\dagger}|0\rangle$ are quite delocalized *within* the 7×7 unit cell. This would then also explain why no temperature dependence is observed for the effective mass m^* due to electron-phonon coupling (the small-polaron problem). Alternatively, there might be important many-body effects, as discussed by Louis *et al.*,[21] which can introduce a finite density of states at the Fermi energy, even for the Hubbard Hamiltonian (25). In this case one can still apply the theory presented above if n and m^* are interpreted as the quasiparticle density and effective mass, respectively, as obtained from the one-particle self-energy $\Sigma(\omega,\vec{q}_{||})$ in the usual way.

IX. SHAPE AND TEMPERATURE DEPENDENCE OF THE QUASIELASTIC PEAK (GENERAL)

In Sec. VII we calculated the shape of the quasielastic peak using (9). Equation (9) is quite complicated and it would be useful to have a simple formula from which one can estimate the width without any extensive numerical calculation. Here we will derive a simple expression for

$$\langle(\Delta\omega)^2\rangle=\langle\omega^2\rangle-\langle\omega\rangle^2 ,$$

where

$$\langle\omega\rangle=\int d\omega\,\omega P(\omega)\equiv\langle\omega\rangle_P .$$

We first rewrite (9) as

$$\int d\omega\,P(\omega)e^{i\omega t}=\exp\left[\int_0^\infty d\omega\,P_s(\omega)[(n_\omega+1)(e^{i\omega t}-1)+n_\omega(e^{-i\omega t}-1)]\right] .$$

Next we expand both sides of this equation in powers of t:

$$1+it\int_{-\infty}^{\infty}d\omega\,\omega P(\omega)-\frac{t^2}{2}\int_{-\infty}^{\infty}d\omega\,\omega^2P(\omega)+\cdots$$
$$=1+it\int_0^\infty d\omega\,\omega P_s(\omega)-\frac{t^2}{2}\left[\int_0^\infty d\omega\,\omega^2P_s(\omega)(2n_\omega+1)+\left[\int_0^\infty d\omega\,\omega P_s(\omega)\right]^2\right]+\cdots .$$

Thus, identifying the coefficients in front of t and t^2,

$$\langle\omega\rangle_P=\langle\omega\rangle_{P_s},\quad \langle\omega^2\rangle_P=\langle\omega^2(2n_\omega+1)\rangle_{P_s}+(\langle\omega\rangle_{P_s})^2 ,$$

so that

$$\langle\omega^2\rangle_P-(\langle\omega\rangle_P)^2=\langle\omega^2(2n_\omega+1)\rangle_{P_s} ,$$

or

$$\langle(\Delta\omega)^2\rangle=\int_0^\infty d\omega\,P_s(\omega)\omega^2(2n_\omega+1) . \tag{24}$$

We will illustrate the usefulness of this equation with two examples. Consider a two-dimensional electronic system on top of a semi-infinite dielectric. Assume that Img is well approximated by

$$\mathrm{Im}g=-\,\mathrm{Im}\frac{2}{\epsilon+1-4\pi ne^2q_{||}/[m^*\omega(\omega+i/\tau)]} , \tag{25}$$

which is identical to (19), except that we now have included a finite relaxation time τ to account for Drude damping within the two-dimensional electronic system. Substituting (25) in (3) gives, after some simplifications (see Appendix A),

$$P_s(\omega)=\frac{C}{\pi\hbar\omega}\int_0^\infty dx\, f(x,\alpha)\frac{1/\beta\tau}{(1/\beta\tau)^2+(\omega/\beta-x)^2}\ , \tag{26}$$

where, as before,

$$C=\frac{4}{\pi}\frac{1}{\cos^2\alpha}\frac{1}{ka_0}\frac{1}{\epsilon+1} \tag{21}$$

and

$$f(x,\alpha)=\frac{1}{x}\int_0^{2\pi} d\phi\left[1+\left[\frac{1/x}{\cos\alpha}-\tan\alpha\cos\phi\right]^2\right]^{-2}\ . \tag{22}$$

Note that

$$\frac{1}{\pi}\frac{1/\beta\tau}{(1/\beta\tau)^2+(\omega/\beta-x)^2}\to\delta(\omega/\beta-x)$$

as $\tau^{-1}\to 0$, so that (26) reduces to (20) when $\tau^{-1}\to 0$.

Substituting (26) in (24), and changing the integration variable $\omega=\beta y$, gives

$$\langle(\hbar\Delta\omega)^2\rangle=\frac{C}{\pi}(\hbar\beta)^2\int_0^\infty dy\, y(2n_{\beta y}+1)\times\int_0^\infty dx\, f(x,\alpha)\times\frac{1/\beta\tau}{(1/\beta\tau)^2+(x-y)^2}\ .$$

Now, it is easy to see that the y integral diverges (logarithmically) at its upper integration limit. The reason for this divergence is the slowly decaying tail of the loss function P_s with increasing ω. However, if we only consider the temperature-dependent contribution to $\langle(\hbar\Delta\omega)^2\rangle$, then this is finite and given by

$$\langle(\hbar\Delta\omega)^2\rangle_T=\frac{2C}{\pi}(\hbar\beta)^2\int_0^\infty dy\frac{y}{e^{\eta y}-1}\times\int_0^\infty dx\, f(x,\alpha)\times\frac{\xi}{\xi^2+(x-y)^2}\ ,$$

where we have introduced the dimensionless parameters

$$\xi=\frac{1}{\beta\tau},\quad \eta=\frac{\hbar\beta}{k_BT}\ .$$

If we write

$$\langle(\hbar\Delta\omega)^2\rangle_T\equiv\frac{2C}{\pi}(\hbar\beta)^2 g(\xi,\eta,\alpha)\ , \tag{27}$$

then one can easily prove that

$$g\sim\pi^2\cos\alpha(1+\cos^2\alpha)\frac{1}{\eta}\ln\frac{1}{\eta}\quad\text{as }\eta\to 0\ , \tag{28}$$

$$g\sim\frac{1.643}{\eta^2}h(\xi,\alpha)\quad\text{as }\eta\to\infty\ , \tag{29}$$

where

$$h(\xi,\alpha)=\int_0^\infty dx\, f(x,\alpha)\frac{\xi}{\xi^2+x^2}\ . \tag{30}$$

The function $h(\xi,\alpha)$ is shown in Fig. 8 and Table II for several α values. Equation (28) shows that, for $\eta\ll 1$, i.e., $\hbar\beta\ll k_BT$,

$$\langle(\Delta\omega)^2\rangle_T\propto T\ln T\ , \tag{31}$$

while for $\eta\gg 1$, i.e., $\hbar\beta\gg k_BT$,

$$\langle(\Delta\omega)^2\rangle_T\propto T^2\ . \tag{32}$$

Thus the temperature dependence of $\langle(\Delta\omega)^2\rangle_T$ is different in the two limiting cases which can be used to distinguish between them. For example, we have found for Si(111)-7×7 (see Fig. 6) that the temperature dependence of the width of the quasielastic peak is weaker than linear at higher temperatures, which is consistent with (31). On the other hand, for a thin metal layer on top of an insulator or semiconductor, one has $\hbar\beta\sim 1$ eV (see next section), so that $\hbar\beta\gg k_BT$. Thus for this system one expects from (32) that the peak width increases linearly with temperature for large temperatures. As discussed later, this is exactly what we find experimentally for thin Au and Pd layers on top of Si(111).

Note that for $\hbar\beta\ll k_BT$, $\langle(\Delta\omega)^2\rangle_T$ is *independent* of the Drude damping $1/\tau$, while in the other case, when $\hbar\beta\gg k_BT$, $\langle(\Delta\omega)^2\rangle_T\to 0$ as $1/\tau\to 0$. This indicates that the physical origin of the broadening is different in the two limiting cases. Indeed, for $\hbar\beta\ll k_BT$ the broadening is caused by multiple excitation of low-frequency plasma oscillations in the two-dimensional electronic system, while for $\hbar\beta\gg k_BT$ the broadening instead arises entirely from the Drude damping and thus vanishes as $1/\tau\to 0$. We will now present numerical results which illustrate these points. Let us first set $1/\tau=0$ and study how the quasielastic peak changes with the parameter β. Assume that $T=230$ K ($k_BT\simeq 20$ meV). The solid lines in Fig. 9 show $P(\omega)$ for three different values of β. The dashed lines show the single-scattering probability $P_s(\omega)$, which agrees with $P(\omega)$ for $\hbar\omega\gtrsim 30$ meV, i.e., for $\hbar\omega\gtrsim 1.5k_BT$. The quasielastic peak has, for $\hbar\beta\ll k_BT$, an approximately Gaussian shape with a width which varies with β as shown in Fig. 10. As β is increased towards $\hbar\beta\approx k_BT$, a no-loss line starts to intensify, while the loss structure

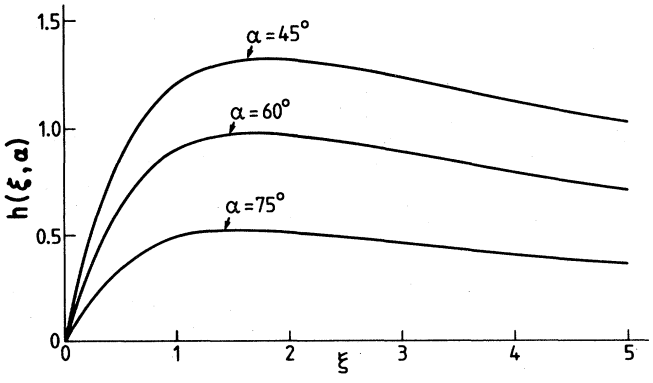

FIG. 8. Function $h(\xi,\alpha)$, defined in (30), shown for three different angles of incidence, $\alpha=45°$, 60°, and 75°.

TABLE II. Values of $h(\xi,\alpha)$ for several different α.

ξ	$h(\xi,\alpha)$ $\alpha=45°$	$\alpha=60°$	$\alpha=75°$
0.2	0.416	0.300	0.158
0.4	0.738	0.542	0.290
0.6	0.964	0.717	0.388
0.8	1.112	0.834	0.454
1.0	1.216	0.908	0.494
1.2	1.277	0.952	0.516
1.4	1.313	0.974	0.526
1.6	1.331	0.983	0.528
1.8	1.336	0.982	0.525
2.0	1.333	0.975	0.518
2.5	1.303	0.941	0.494
3.0	1.257	0.899	0.467
3.5	1.207	0.855	0.440
4.0	1.158	0.813	0.416
5.0	1.065	0.738	0.373
6.0	0.984	0.675	0.338
9.0	0.801	0.539	0.266
12.0	0.679	0.451	0.221
15.0	0.592	0.390	0.190
18.0	0.526	0.346	0.167
21.0	0.475	0.311	0.149
24.0	0.434	0.283	0.135
27.0	0.400	0.260	0.124
30.0	0.371	0.241	0.115

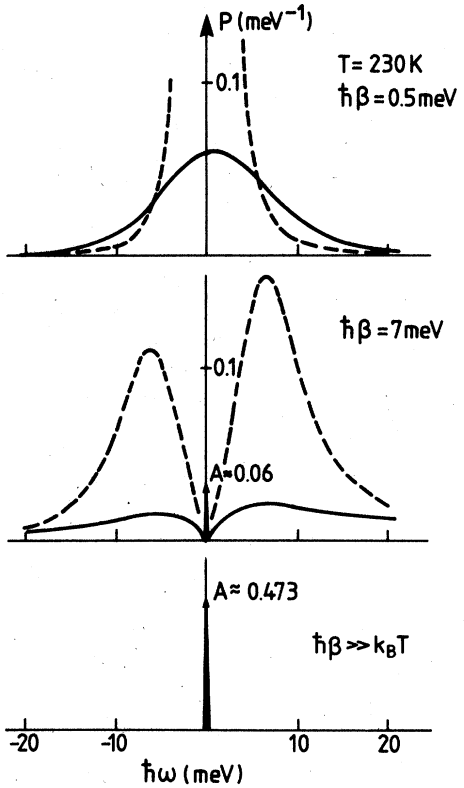

FIG. 9. Loss probability $P(\hbar\omega)$ at $T=230$ K is shown for $\hbar\beta=0.5$, 7 meV, and $\hbar\beta\gg k_BT$. The dashed line is the single-scattering "probability" which agrees with the multiple-scattering probability (solid line) for $\hbar\omega\gtrsim 30$ meV. $1/\tau=0$, $E_0=12$ eV, and $\alpha=45°$.

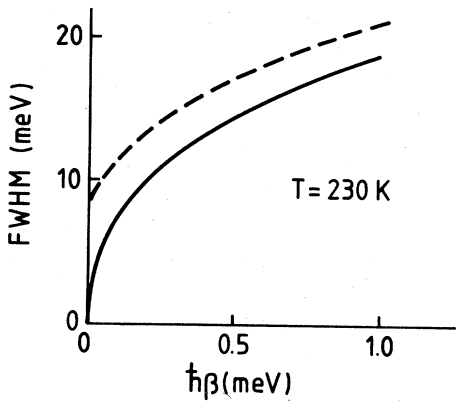

FIG. 10. Full width at half maximum of the quasielastic peak shown as a function of $\hbar\beta$ for $T=230$ K. The solid and dashed curves are the results before and after convolution with a Gaussian with a FWHM of 8.4 meV. $E_0=12$ eV and $\alpha=45°$.

splits into a gain part and a loss part which both move towards larger $|\omega|$ as β increases. If we write

$$P(\omega)=A\delta(\hbar\omega)+B(\omega)\ ,$$

then the weight A of the no-loss line is given by [see Eq. (8)]

$$A=\exp\left[-\int_0^\infty d\omega\, P_s(\omega)(2n_\omega+1)\right]\ .$$

The variation of A with β is shown in Fig. 11 (again for $E_0=12$ eV and $\alpha=45°$ in all the numerical calculations). We note that $A\simeq 0$ for $\hbar\beta\ll k_BT$, while $A\simeq 0.47$ for $\hbar\beta\gg k_BT$. Thus, for $\hbar\beta\gg k_BT$, the loss spectrum $P(\omega)$ in the absence of Drude damping will consist of a $\delta(\hbar\omega)$ contribution carrying about 50% of the incident electrons in addition to a loss contribution $B(\hbar\omega)$ centered at $\hbar\omega\sim\hbar\beta$ and caused by excitation of undamped plasmons.

Some aspects of the behavior of $P(\omega)$ as a function of β, shown in Fig. 9, can be understood as follows. The dispersion relation for two-dimensional plasmons is given by the pole of $g(q_{||},\omega)$, i.e.,

$$\hbar\omega=(2E_0\hbar\beta q_{||}/k_0)^{1/2}\ .$$

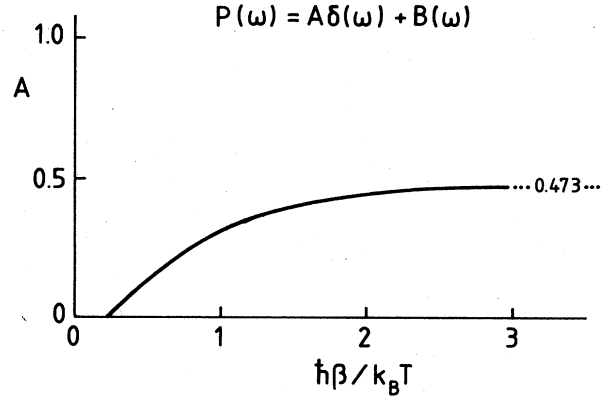

FIG. 11. Weight A of the no-loss line shown as a function of $\hbar\beta/k_BT$. $E_0=12$ eV and $\alpha=45°$.

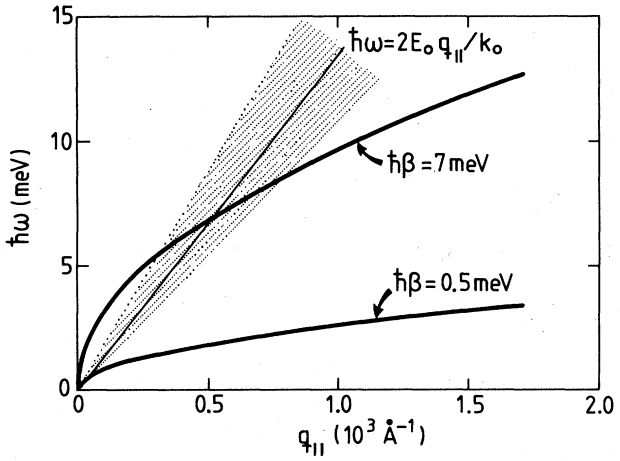

FIG. 12. Dotted area shows the region in the $(\omega,q_{||})$ plane where the kinematic dipole scattering prefactor takes its largest value (schematically). The other two curves show the dispersion relation of two-dimensional plasmons $[\hbar\omega=(2E_0\hbar\beta q_{||}/k_0)^{1/2}]$ with $\hbar\beta=0.5$ and 7 meV, respectively. $E_0=12$ eV.

In Fig. 12 this dispersion relation is shown for $\hbar\beta=0.5$ and 7 meV. The electric field from an incident electron contains all possible $q_{||}$, and can therefore excite any of the two-dimensional plasmons without violating the momentum-conservation law. However, the kinematics of dipole scattering is such that the largest fraction of the inelastically scattered electrons has transferred a momentum $q_{||}\sim k_0\hbar\omega/2E_0$ to the excitations in the substrate (the dotted area in Fig. 12). Thus one expects to find a peak in the inelastic scattering probability $P(\omega)$ when the surface-plasmon dispersion curve overlaps the dotted area in Fig. 12. For $\hbar\beta=7$ meV this occurs at $\hbar\omega\approx 7$ meV, in good agreement with Fig. 9. For $\hbar\beta=0.5$ meV it occurs at $\hbar\omega\approx 1$ meV, thus falling within the broadened quasielastic peak.

Let us now introduce a finite Drude damping $1/\tau$. This will broaden the $\delta(\hbar\omega)$ function in Fig. 9 into an approximately Lorentzian function (see Appendix D):

$$P(\omega)\approx\frac{1}{\pi}\left[\frac{\Gamma/2}{\omega^2+(\Gamma/2)^2}\cos\phi+\frac{\omega}{\omega^2+(\Gamma/2)^2}\sin\phi\right], \quad (33)$$

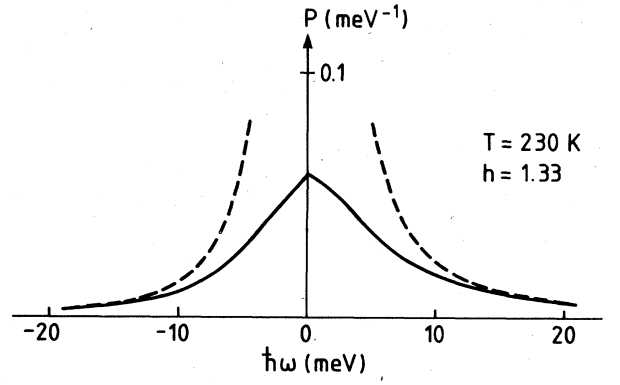

FIG. 13. Loss probability $P(\hbar\omega)$ for $T=230$ is shown for $h=1.33$, $E_0=12$ eV, and $\alpha=45°$.

where $\Gamma=2Ch(1/\beta\tau,\alpha)k_BT$ and $\phi=Ch(1/\beta\tau,\alpha)/2$. On the gain side, this equation, is valid only as long as $P(\omega)>0$. In deriving (33) it has been assumed that $\phi\ll 1$. The second term in $P(\omega)$ gives rise to the expected asymmetry between the gain and loss sides of the spectrum. Note that $P(\omega)$ only depends on *one* material parameter, $h(\xi,\alpha)$. Furthermore, as a function of $\xi=1/\beta\tau$, h and, thus, the FWHM $\approx\Gamma$ as well, has a *maximum* at $\xi\approx 2$, as seen in Fig. 8. Figure 13 shows $P(\omega)$ for $T=230$ K and $h=1.33$.

X. CONDUCTIVITY PROPERTIES OF THIN METAL FILMS ON Si(111)

In this section we will study the conductivity properties of thin Au and Pd overlayers on Si(111). These data will be analyzed using the theory outlined above.

For a thin metal overlayer, we have

$$\hbar\beta=\frac{4\pi ne^2}{m^*}\frac{m}{(\epsilon+1)k}\equiv\omega_P^2 d\frac{m}{(\epsilon+1)k}\ . \quad (34)$$

Here, $n=dN/V$ where N/V is the number of conduction electrons per unit volume of the metal and d is the film thickness. m^* is the effective mass for an electron on the Fermi surface. Considering Au, we would determine $\hbar\beta(\text{Au})\simeq 0.48d$, where $\hbar\beta$ is measured in electron volts and d in angstroms. Thus for most physically realizable metal *films* ($d\gtrsim 2$ Å), we have $\hbar\beta\gg k_BT$, and, as discussed in the last section, the broadening of the quasielastic peak is entirely due to Drude damping and depends only on $\xi=1/\beta\tau$. The film resistivity ρ can be obtained from

$$\rho=\frac{d\xi}{(\epsilon+1)\epsilon_0 v}\ \text{(SI units)}\ , \quad (35)$$

where ϵ_0 is the dielectric permeability of vacuum and v is the velocity of the incident electrons.

We first consider the equivalent of 8.5 Å of Au evaporated at room temperature on top of Si(111). It was found experimentally that the broadening of the quasielastic peak was maximal for this film thickness, and from the discussion in the preceding section we therefore know without any further calculation that $\xi=1/\beta\tau\approx 2$. Figure 14 shows $P(\omega)$ for three different temperatures, $T=55$, 180, and 223 K. The solid lines in Fig. 14 represent the theoretical result calculated from the equations given in Appendix D with $\xi=2$. The agreement between theory and experiment is remarkably good if one realizes that there is no fitting parameter in the theory. [Here, $P(\omega)$ depends only on the (known) material parameter ξ.] The only disagreement between theory and experiment occurs on the gain side for $\hbar\omega\gtrsim 7$ meV, where the experimental data points are located above the theoretical curve. Again, this can be attributed to an alignment problem of the spectrometer. The circles in Fig. 15 show in greater detail the temperature dependence of the FWHM. The agreement between theory (solid curve) and experiment is again good. Using the known value of $\xi=2$ we calculate a film resistivity of $\rho(\text{film})\simeq 660\ \mu\Omega$ cm for this Au film. A Au crystal at room temperature (RT) has a resistivity $\rho\approx 2\ \mu\Omega$ cm, while the resistivity of liquid Au at T

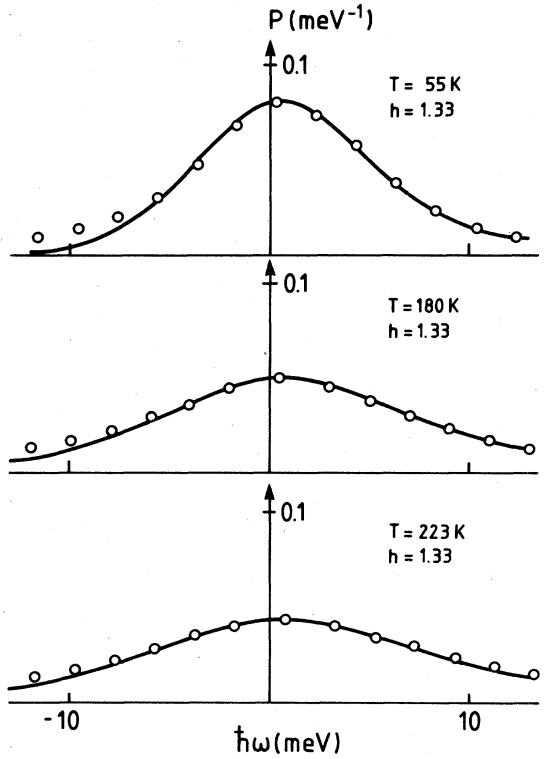

FIG. 14. Loss probability $P(\hbar\omega)$ from a 8.5-Å-thick Au film for three different temperatures, $T=223$, 180, and 55 K. The open circles represent the experimental data for $E_0=12$ eV and $\alpha=45°$.

$=1500$ K is $\rho\approx 32\ \mu\Omega$ cm.

We have also studied the conductivity properties of thin Pd layers on top of Si(111). In this case it is believed that Pd evaporated at RT on Si(111) forms a metallic silicide layer, Pd_2Si, on the surface. Figure 16 shows the results for 10 Å of Pd evaporated onto Si(111), forming a 14-Å-thick Pd_2Si film. The open and solid circles represent the experimental results without and with adsorbed hydrogen, respectively. The solid curve is the result of a theoretical calculation with $h=1.17$ corresponding to $\xi=0.9$. There is good agreement between theory and experiment. Note that the hydrogen-saturated film has almost the same conductivity as the film without hydrogen. With $\xi=0.9$ and $d=14$ Å we calculate $\rho=554\ \mu\Omega$ cm, while for a bulk Pd_2Si crystal at room temperature, $\rho\simeq 25\ \mu\Omega$ cm.[22]

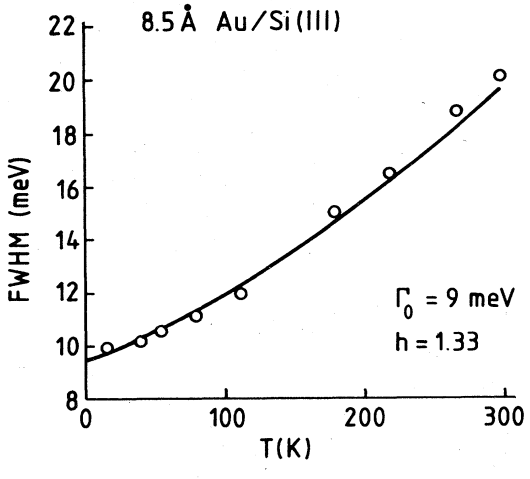

FIG. 15. Temperature dependence of the peak width (full width at half maximum) of the quasielastic peak from a 8.5-Å-thick Au layer on top of Si(111). The open circles denote the experimental data and the solid line denotes the result of a theoretical calculation with $h=1.33$ and $\Gamma_0=9$ meV (Γ_0 is the FWHM of the instrumental resolution function taken as a Gaussian).

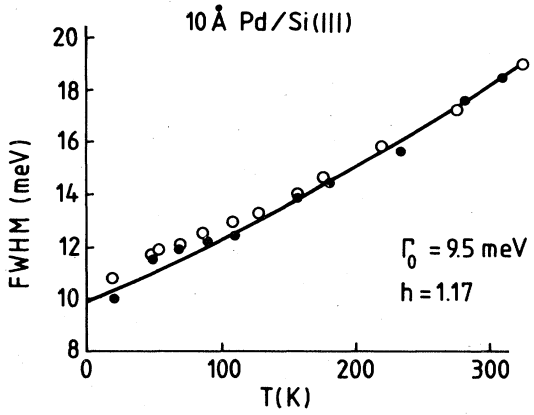

FIG. 16. Temperature dependence of the peak width (full width at half maximum) of the quasielastic peak from a 14-Å-thick Pd_2Si layer on Si(111). The open and solid circles represent the experimental data without and with adsorbed hydrogen, respectively. The solid line is the result of a theoretical calculation with $h=1.17$ and $\Gamma_0=9.5$ meV.

Before we discuss the structural implications of the results presented above, let us briefly discuss the measurements by Dubois *et al.*[7] on thin Ag films on GaAs. The Ag films were grown and studied at $T=170$ K. The width of the quasielastic peak for film thicknesses $d=1.7$, 2.5, 3.4, and 17 Å was found to be 9.5, 16, 11.3, and 6.5 meV, respectively. The instrumental resolution was $\Gamma_0=6.5$ meV, $E_0=5$ eV, and $\alpha=60°$. Using the theory above we calculate the film resistivities (in $\mu\Omega$ cm) as follows (with d in angstroms):

$$\rho=2583 \quad \text{for } d=1.7\ ,$$

$$\rho=94 \quad \text{for } d=2.5\ ,$$

$$\rho=62 \quad \text{for } d=3.4\ .$$

A Ag crystal at $T=170$ K has a resistivity $\rho\simeq 1\ \mu\Omega$ cm, while the resistivity of liquid Ag at $T\simeq 1500$ K is $\rho\approx 20\ \mu\Omega$ cm. Thus the silver films have an even larger resistivity than liquid Ag. To understand the physical origin of this, and, in particular, the particularly large resistivity of the $d=1.7$ Å Ag film, let us first note that from various measurements it is known that Ag films grown at $T=170$ K are "uniform" [the diffusivity of Ag atoms, and thus the tendency to form large clusters (bumps), at this low temperature, is small]. Figure 17 shows a possible configuration of Ag atoms on GaAs for the $d=1.7$ Å film. This figure is constructed by randomly distributing 72 Ag atoms among the lattice sites of a hexagonal lattice with 100 sites, and with a nearest-neighbor distance equal

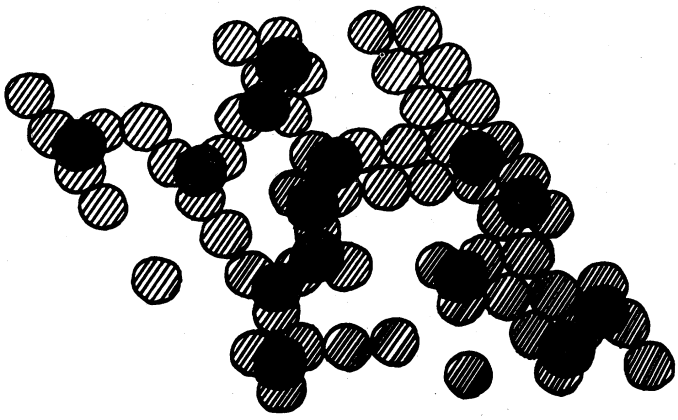

FIG. 17. Possible configuration of Ag atoms for a 1.7-Å-thick film of Ag on GaAs.

to that in bulk silver ($\simeq$2.89 Å). This number of Ag atoms per unit area corresponds to a 1.7-Å-thick Ag film. The hatched circles represent the Ag atoms adsorbed directly on the GaAs substrate, while the solid circles represent Ag atoms absorbed on top of the first layer of Ag atoms. The effective coverage (defined as the ratio of lattice sites occupied by hatched circles to the total number of lattice sites) is $\theta=0.58$. This is close to the (site-) percolation threshold which, for a hexagonal lattice, is $\theta_c=0.5$. Below the percolation threshold, $\theta<\theta_c$, the resistivity is infinite, $\rho=\infty$. Thus the high resistivity of the $d=1.7$ Å film can be attributed to the fact that this film is just above the percolation threshold where a very low concentration of connected (and thus conducting) paths exist in the film. The relatively high resistivities of the $d=2.5$ and 3.4 Å films are probably, in part, caused by the same phenomenon, because one would expect the Drude damping (elastic scattering of electrons from lattice imperfections) to be similar, for these films to liquid Ag. When the low-temperature-deposited Ag films were slowly warmed to room temperature overnight, most of the broadening disappeared, which Dubois *et al.* interpreted as the growth of metal islands (bumps) separated by areas of almost uncovered GaAs. We point out that the dipole scattering theory is valid for such inhomogeneous systems if the inhomogeneities are small and uniform relative to $q_{\|}^{-1}$. [Recall that our studies of the quasielastic peak involve $q_{\|}\sim 10^{-4}$ Å and the response of the metal film to the slowly varying components $\phi_{\rm ext}\sim \exp(i\vec{q}_{\|}\cdot\vec{x}_{\|})$ of the potential from the external electron.] Thus our analysis provides the resistivity of an "effective" homogeneous film whose average resistivity can be related to its actual microstructure—which, in general, can be very complicated.

As pointed out above, Pd on Si(111) tends to form Pd_2Si already at room temperature. From various measurements it has been concluded that these Pd_2Si films are very uniform.[23] The rather large resistivity, $\rho=550$ $\mu\Omega$ cm, for this film is therefore likely caused by diffuse scattering at the Pd_2Si film boundaries. A simple free-electron theory can be used to estimate this, and it predicts[24]

$$\rho(\text{film})\approx\rho(\text{bulk})\frac{4/3}{(d/l_0)\ln(l_0/d)},\quad d\ll l_0 \tag{36}$$

where l_0 is the bulk mean free path in Pd_2Si. Using $\rho(\text{bulk})=25$ $\mu\Omega$ cm and $l_0=220$ Å (Ref. 22) gives $\rho(\text{film})\approx 200$ $\mu\Omega$ cm, which is rather close to the observed film resistivity. We note that diffuse scattering at the surfaces cannot explain the large resistivity of the gold film since Eq. (36) would predict a film resistivity of $\rho(\text{film})\approx 33$ $\mu\Omega$ cm, which is still well below what we observe. The large resistivity of the Au films can arise from either the occurrence of Au bumps or the formation of a Au-Si surface compound with its own intrinsically higher resistivity.

XI. SUMMARY AND CONCLUSION

We have presented a detailed discussion of the nature of the quasielastic peak for electrons scattered from a variety of interesting physical systems. Illustrative applications were given for the 7×7 reconstructed Si(111) surface and thin metallic layers on Si(111). We have shown that from studies of the temperature dependence of the width (FWHM) of the quasielastic peak it is often possible to obtain detailed information regarding surface free carriers and surface conductivities as well as models for the electronic structure of surfaces.

We expect that the unique ability of EELS to provide such information will stimulate a wide range of studies, ranging from studies of surface defects and surface conductivity of semiconductor surfaces to studies of phase transitions in the transition-metal dichalcogenides.

ACKNOWLEDGMENTS

We would like to thank U. Backes, H. Froitzheim, H. Ibach, and K. C. Pandey for useful discussions, and to acknowledge the U. S. Office of Naval Research for partial support of this work.

APPENDIX A

In this appendix we will prove (26).

Since $\hbar\omega\ll E_0$ we have $k\approx k'$, and from (3) we obtain

$$P_s(\omega)=\frac{2}{(ea_0\pi)^2}\frac{1}{\cos\alpha}\int d\Omega_{k'}\frac{q_{\|}}{|q_{\|}^2+q_{\perp}^2|^2}\,\mathrm{Im}g(q_{\|},\omega)\ . \tag{A1}$$

The integral in (A1) is of the form

$$\int d\Omega_{k'} f(q_{\|},q_{\perp})$$

and can be evaluated as follows: Energy conservation gives

$$\frac{\hbar^2k^2}{2m}=\frac{\hbar^2k'^2}{2m}+\hbar\omega\ ,$$

or

$$k'=(k^2-2m\omega/\hbar)^{1/2}\approx k-\omega/v\ ,$$

where $v=\hbar k/m$ is the velocity of the incident electron. Thus,

$$\int d\Omega_{k'} f(q_{||},q_\perp) \approx \int d^3k' f(q_{||},q_\perp)\delta(k'-k+\omega/v)/k^2 . \tag{A2}$$

Since $\vec{k}=\vec{k}'+\vec{q}$ we obtain $k'\approx k-\vec{q}\cdot\vec{k}/k$. Changing the integration variable from $\vec{k}'$ to $\vec{q}$ in (A2) gives

$$\int d\Omega_{k'} f(q_{||},q_\perp) \approx \frac{1}{k^2}\int d^3q\, f(q_{||},q_\perp)\delta(\vec{q}\cdot\hat{k}-\omega/v) ,$$

where $\hat{k}=\vec{k}/k$. Since

$$\vec{q}\cdot\hat{k}=q_{||}\cos\phi\sin\alpha+q_\perp\cos\alpha ,$$

we obtain

$$\int d\Omega_{k'} f(q_{||},q_\perp)=\frac{1}{k^2}\int d^2q_{||}dq_\perp f(q_{||},q_\perp)\delta(q_{||}\cos\phi\sin\alpha+q_\perp\cos\alpha-\omega/v)$$

$$=\frac{1}{k^2}\int d^2q_{||} f\left(q_{||},\frac{\omega/v}{\cos\alpha}-q_{||}\tan\alpha\cos\phi\right)\frac{1}{\cos\alpha} .$$

Thus we can write (A1) as

$$P_s(\omega)=\frac{2}{(ea_0\pi)^2}\frac{1}{k^2\cos^2\alpha}\int d^2q_{||}q_{||}\left[q_{||}^2+\left[\frac{\omega/v}{\cos\alpha}-q_{||}\tan\alpha\cos\alpha\right]^2\right]^{-2}\mathrm{Img}(q_{||},\omega) .$$

We define [see Eq. (22)]

$$f(x,\alpha)=\frac{1}{x}\int_0^{2\pi} d\phi\left[1+\left[\frac{1/x}{\cos\alpha}-\tan\alpha\cos\phi\right]^2\right]^{-2} ,$$

so that

$$P_s(\omega)=\frac{2}{(ea_0\pi)^2}\frac{1}{k^2\cos^2\alpha}\frac{v}{\omega}\int dq_{||}\frac{1}{q_{||}}\times f\left(\frac{vq_{||}}{\omega},\alpha\right)\mathrm{Img}(q_{||},\omega) , \tag{A3}$$

or if $vq_{||}/\omega=x$ is introduced as a new integration variable,

$$P_s(\omega)=\frac{2}{(ea_0\pi)^2}\frac{1}{k^2\cos^2\alpha}\frac{v}{\omega}\int dx\frac{1}{x}f(x,\alpha)\times\mathrm{Img}\left(\omega\frac{x}{v},\omega\right) . \tag{A4}$$

To proceed, Img must be specified. Assume that Img is given by (25). Introducing

$$\beta=\frac{4\pi ne^2}{m^*(\epsilon+1)}\frac{1}{v} ,$$

we obtain

$$P_s(\omega)=\frac{C}{\pi}\frac{1}{\hbar\omega}\int_0^\infty dx\, f(x,\alpha)\frac{1/\beta\tau}{(1/\beta\tau)^2+(\omega/\beta-x)^2} ,$$

which is identical to (26).

APPENDIX B

In this appendix we will discuss the contribution from phonons to the width of the quasielastic peak.

By inversion symmetry, the long-wavelength lattice-vibrational modes in bulk silicon have zero dynamical dipole moment. Now, at a surface of a silicon crystal this symmetry is broken; thus surface silicon atoms have nonzero dynamical dipole moments.[10,20] This makes it possible to excite both bulk and surface phonons using inelastic electron scattering. The surface phonons cannot broaden the quasielastic peak since they occur at discrete loss energies $\hbar\omega_1$, $\hbar\omega_2$, ... We will now prove that bulk-phonon excitation cannot broaden the quasielastic peak either. Since the momentum transfer, $\hbar\vec{q}_{||}$, in EELS, from low-energy excitations, is negligible, only bulk phonons with $q_{||}\simeq 0$ can broaden the quasielastic peak. (Bulk phonons with $\vec{q}_{||}\approx\vec{G}$, where $\vec{G}$ is a reciprocal-lattice vector of the *surface* lattice structure, can also be excited, but cannot broaden the quasielastic peak since they have finite frequencies.) Thus we need only to consider bulk phonons which propagate normal or almost normal to the Si(111) surface. We have, therefore, a one-dimensional problem for the phonon dynamics which can be solved analytically. Following the same procedure as described elsewhere, we can derive[25]

$$(\mathrm{Img})_{\mathrm{phonon}}=\frac{4}{\sqrt{3}}\frac{q_{||}a}{(\epsilon+1)^2}\left[\frac{e^*}{e}\right]^2\left[\frac{\omega_{\mathrm{ion}}}{\omega_0}\right]^2\mathrm{Im}f(\omega) ,$$

where

$$\omega_{\mathrm{ion}}=[4\pi e^2/(Ma^3/8)]^{1/2} ,$$

$a=5.43$ Å is the Si lattice constant, ω_0 is the highest longitudinal-phonon frequency in the [111] direction, and e^* is an effective charge. The function f is given by

$$f(\omega)=1+4\bar{\omega}^2-8\bar{\omega}^4+i\,8\bar{\omega}^3(1-\bar{\omega}^2)^{1/2} .$$

We have introduced $\bar{\omega}=\omega/\omega_0$. Now, as $\omega\to 0$, $\mathrm{Im}f\to 8\bar{\omega}^3$. Thus, $n_\omega P_s(\omega)\sim\omega$ as $\omega\to 0$, implying that bulk phonons cannot broaden the quasielastic peak.

The following reservation must be added to the discussion above: If there is a very-low-energy surface phonon

($\hbar\omega_1 \simeq 1$ meV), then owing to the finite resolution of EEL spectrometers, it would be impossible to resolve the individual surface-phonon—loss peaks, which therefore would broaden the quasielastic peak. However, there is no reason for expecting such a "soft" surface phonon on the Si(111)-7×7 surface.

APPENDIX C

In this appendix we will discuss the influence of a low density of free bulk carriers on the quasielastic peak. We will first assume that the carrier concentration is a constant up to the Si-vacuum interface, i.e., that there is no band bending. The bulk dielectric function is taken to be

$$\epsilon(\omega)=\epsilon_b-\frac{\omega_P^2}{\omega(\omega+i/\tau)} ,$$

where $\omega_P^2=4\pi ne^2/m^*$, with n the concentration of carriers with effective mass m^*. We find if $1/\tau$ is infinitesimal,

$$\mathrm{Im}g=\mathrm{Im}\frac{\epsilon-1}{\epsilon+1}=\frac{\pi}{\epsilon_b+1}\bar{\omega}_P\delta(\omega-\bar{\omega}_P) ,$$

where

$$\bar{\omega}_P=\omega_P(\epsilon_b+1)^{-1/2} .$$

Substituting this into (A4) gives

$$P_s(\omega)=\frac{C}{2}\delta(\omega-\bar{\omega}_P)\int_0^\infty dx\frac{1}{x}f(x,\alpha) . \tag{C1}$$

The integral in this expression is evaluated as follows: We have

$$\int_0^\infty dx\frac{1}{x}f(x,\alpha)=\int_0^\infty dx\frac{1}{x^2}\int d\phi\left[1+\left[\frac{1/x}{\cos\alpha}-\tan\alpha\cos\phi\right]^2\right]^{-2} .$$

Substituting $1/(x\cos\alpha)=y$ on the right-hand side gives the integral

$$\int_0^\infty dy\int d\phi\frac{\cos\alpha}{[1+(y-\tan\alpha\cos\phi)^2]^2}\equiv\cos\alpha\frac{d}{d\xi}F(\xi)\Big|_{\xi=1} ,$$

where

$$F(\xi)=\int_0^\infty dy\int d\phi\frac{-1}{\xi+(y-\tan\alpha\cos\phi)^2}=\tfrac{1}{2}\int_{-\infty}^\infty dy\int d\phi\frac{-1}{\xi+(y-\tan\alpha\cos\phi)^2} .$$

Closing the y integration in the upper half of the complex y plane gives

$$F(\xi)=\tfrac{1}{2}\left[2\pi i\int d\phi\frac{-1}{2i\sqrt{\xi}}\right]=-\pi^2/\sqrt{\xi} .$$

Thus

$$\int_0^\infty dx\frac{1}{x}f(x,\alpha)=\cos\alpha\frac{d}{d\xi}\frac{-\pi^2}{\sqrt{\xi}}\Big|_{\xi=1}=\frac{\pi^2}{2}\cos\alpha .$$

Substituting this into (C1) gives

$$P_s(\omega)=\frac{C\pi^2}{4}\delta(\omega-\bar{\omega}_P)\cos\alpha . \tag{C2}$$

Substituting (C2) into (9) gives

$$P(\omega)=\frac{1}{2\pi}\int dt\,e^{-i\omega t}e^{F(t)} , \tag{C3}$$

where

$$F(t)=\frac{C\pi^2\cos\alpha}{4}[(n_{\bar{\omega}_p}+1)(e^{i\bar{\omega}_P t}-1)+n_{\bar{\omega}_P}(e^{-i\bar{\omega}_P t}-1)] .$$

From (C3), $P(\omega)$ is easily obtained by numerical integration. Using (26) and (C2) it is possible to calculate $\langle(\Delta\omega)^2\rangle$ analytically:

$$\langle(\Delta\omega)^2\rangle=\frac{C}{4}\pi^2\bar{\omega}_P^2\left[\frac{2}{e^{\hbar\bar{\omega}_P/k_BT}-1}+1\right]\cos\alpha .$$

If $\hbar\bar{\omega}_P \ll k_BT$, then

$$\langle(\hbar\Delta\omega)^2\rangle\simeq\frac{C}{2}\pi^2\hbar\bar{\omega}_P k_BT\cos\alpha . \tag{C4}$$

This should be compared with

$$\langle(\hbar\Delta\omega)^2\rangle\simeq 2C\pi\cos\alpha(1+\cos^2\alpha)\hbar\beta k_BT\ln(k_BT/\hbar\beta) , \tag{C5}$$

which is the broadening in a two-dimensional electronic system when $\hbar\beta \ll k_BT$ [see Eq. (28)]. The ratio between (C4) and (C5) is

$$\frac{\pi}{4(1+\cos^2\alpha)}\frac{\hbar\bar{\omega}_P}{\hbar\beta}\frac{1}{\ln(k_BT/\hbar\beta)} .$$

With a boron doping of 1.3×10^{15} atoms/cm^3 and $m^*\simeq 0.16m_e$, one obtains $\hbar\bar{\omega}_P\approx 1$ meV. With $\hbar\beta=0.2$ meV the above ratio is approximately equal to 0.5 at room temperature. Thus, if there were no band bending one would expect the free bulk carriers (holes) to give an important contribution to the broadening of the quasielastic peak in the present case. However, it is known that the separation between the Fermi energy E_F and the valence-band top at the surface of Si(111)-7×7 is[20] $E_F-E_v(\text{surface})\simeq=0.51$ eV. For a p-type doping, $N_A=1.3\times10^{15}$ cm^{-3}, one can calculate

$$E_F-E_v(\text{bulk})\simeq k_BT\ln(N_v/N_A)\simeq 8k_BT=0.2 \text{ eV}$$

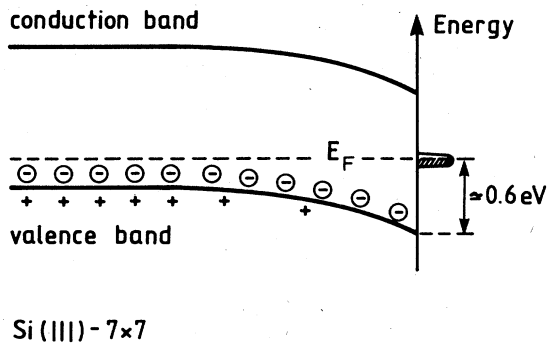

FIG. 18. Band bending in the vicinity of a clean Si(111)-7×7 surface. The bulk-Si crystal is doped with acceptor impurities.

at room temperature. Thus the bands will bend so that there will be a *depletion* of free carriers (holes) in the surface region of Si(111)-7×7; see Fig. 18. Note also that for a hydrogen-covered Si(111) surface, $E_F - E_v$(surface) $\simeq 0.46$ eV, so that this surface has a smaller band bending and thus also a higher concentration of free carriers at the surface. Nevertheless, there is no observable broadening of the quasielastic peak for the hydrogen-covered surface, giving additional support to the idea that the observed broadening on Si(111)-7×7 is an intrinsic surface effect and not due to bulk-derived free carriers in the surface region.

APPENDIX D

We will prove (33). We write (9) as

$$P(\omega)=\frac{1}{2\pi}\int dt\, e^{-i\omega t}e^{F(t)}\,, \tag{D1}$$

where

$$F(t)=\int_0^\infty d\omega' P_s(\omega')[(n_{\omega'}+1)(e^{i\omega' t}-1)+n_{\omega'}(e^{-i\omega' t}-1)]\,. \tag{D2}$$

It was shown in Appendix A that

$$P_s(\omega)=\frac{C}{\pi\hbar\omega}\int_0^\infty dx\, f(x,\alpha)\frac{1/\beta\tau}{(1/\beta\tau)^2+(\omega/\beta-x)^2}\,. \tag{D3}$$

Assume now that $\omega/\beta \ll 1$ (for a metal film a few angstroms thick; for example, $\hbar\beta \sim 1$ eV, while we are interested in $\hbar\omega \lesssim 10$ meV). Equation (D3) then reduces to

$$P_s(\omega)=\frac{C}{\pi\hbar\omega}h(1/\beta\tau,\alpha)\,, \tag{D4}$$

where

$$h(\xi,\alpha)=\int_0^\infty dx\, f(x,\alpha)\frac{\xi}{\xi^2+x^2}\,.$$

The function $h(\xi,\alpha)$ is shown in Fig. 9 for a few different α. Equation (D4) is valid for $\omega \ll \beta$. Substituting (D4) into (D2) and changing the integration variable $\omega' = k_B T x$, we obtain

$$F(t)=\int_0^R \frac{dx}{x}\frac{Ch}{\pi}\left[\left[\frac{1}{e^x-1}+1\right](e^{ixy}-1)+\frac{1}{e^x-1}(e^{-ixy}-1)\right], \tag{D5}$$

where $y = tk_B T$, and where R is a large number (say, $R \sim 20$), but $R \ll \hbar\beta/k_B T$. Now, since

$$\frac{1}{e^x-1}+1=-\frac{1}{e^{-x}-1}\,,$$

we obtain

$$F(t)=\frac{Ch}{\pi}\int_0^R \frac{dx}{x}\left[\frac{-1}{e^{-x}-1}\right](e^{ixy}-1)+\frac{Ch}{\pi}\int_0^R \frac{dx}{x}\frac{1}{e^x-1}(e^{-ixy}-1)\,.$$

Changing the integration variable $x \to -x$ in the second integral gives

$$F(t)=-\frac{Ch}{\pi}\int_{-R}^R \frac{dx}{x}\frac{1}{e^{-x}-1}(e^{ixy}-1)\,. \tag{D6}$$

Note that the integrand in (D5) is finite at $x=0$, while the integrand in (D6) diverges as x^{-1} as $x \to 0$. We must therefore interpret the integral (D6) as a principal integral:

$$\int_{-R}^R = \lim_{\epsilon\to 0}\left[\int_{-R}^{-\epsilon}+\int_\epsilon^R\right].$$

Note also that the integral diverges logarithmically as $R \to \infty$; thus R must be kept finite but large. Equation (D6) is conveniently evaluated using the residue theorem. The integrand has single poles at $x = 2\pi n i$, $n = 0, \pm 1, \pm 2, \ldots$. Consider first $y > 0$ and study the integral

$$H(y)\equiv -\oint_M \frac{dx}{x}\frac{1}{e^{-x}-1}(e^{ixy}-1)\,,$$

where the closed curve M is shown in Fig. 19. The resi-

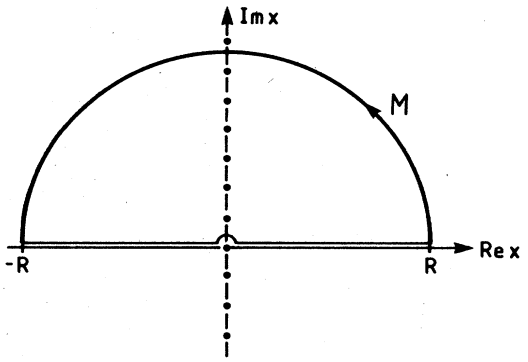

FIG. 19. Solid curve is the integration contour M of the integral H defined in the text.

due theorem gives

$$H(y)=\sum_{n=1}^{N}\frac{1}{n}(e^{-2\pi n|y|}-1)\rightarrow-\ln(1-e^{-2\pi|y|})+\text{const}$$

as $N\rightarrow\infty$. Strictly speaking, N should be chosen as a large but finite number, but for practical purposes one can take $N\rightarrow\infty$ because the exponential series converges very rapidly (for $|y|\gtrsim 0.1$, which are the only important y). For large R it is easy to evaluate the integral over the half-circle M_1 (set $x=Re^{i\phi}$, $\phi\in[0,\pi]$),

$$\int_{M_1}\frac{ax}{x}\frac{-1}{e^{-x}-1}(e^{ixy}-1)=-i\frac{a}{2}\pi .$$

Finally, the integral over the contour M_0 gives (set $x=\epsilon e^{i\phi}$, $\pi>\phi>0$

$$\int_{M_0}\frac{dx}{x}\frac{-1}{e^{-x}-1}(e^{ixy}-1)=i\int_{\pi}^{0}d\phi(iy)=\pi y .$$

Thus,

$$F(t)=\frac{Ch}{\pi}\left[H(y)-\int_{M_1}-\int_{M_0}\right]=\frac{Ch}{\pi}\left[-\ln(1-e^{-2\pi|y|})+i\frac{\pi}{2}\frac{y}{|y|}-\pi|y|\right]+\text{const} . \tag{D7}$$

This equation is valid for $y>0$ as well as $y<0$, as is easily shown by closing the integration contour in the lower half plane when $y<0$.

We have used (D1) and (D7) in all the numerical calculations in this paper. However, if $Ch/\pi\ll 1$, then we can approximate (D7) by

$$F(t)\simeq Ch\left[i\frac{y}{2|y|}-|y|\right] .$$

Substituting this in (C1) gives

$$P(\omega)=\frac{1}{2\pi}\int_{0}^{\infty}dt\,e^{-i\omega t}e^{-Chk_BTt}e^{iCh/2}+\frac{1}{2\pi}\int_{-\infty}^{0}dt\,e^{-i\omega t}e^{Chk_BTt}e^{-iCh/2}$$
$$=\frac{1}{\pi}\left[\frac{\Gamma/2}{\omega^2+(\Gamma/2)^2}\cos\phi+\frac{\omega}{\omega^2+(\Gamma/2)^2}\sin\phi\right] , \tag{D8}$$

where $\Gamma=2Ch(1/\beta\tau,\alpha)k_BT$ and $\phi=Ch(1/\beta\tau,\alpha)/2$. Finally, the measured quasielastic peak is obtained by convoluting $P(\omega)$ with the instrumental resolution function.

APPENDIX E

Here we will give a very simple estimate of the effective mass m^* associated with conduction within a lattice of localized orbitals (e.g., dangling bonds) on the Si(111) surface. Consider first two orbitals $|a\rangle$ and $|b\rangle$ separated by a distance R. The energy levels of these orbitals are located in the silicon bulk band gap, a distance V below the conduction-band edge, as schematically shown in Fig. 20. Suppose now that the orbital $|a\rangle$ contains one electron,

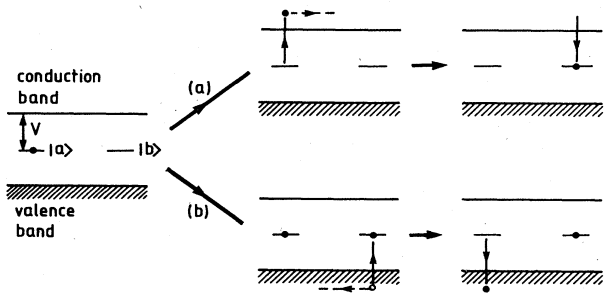

FIG. 20. An electron in a dangling-bond orbital $|a\rangle$ on the Si(111) surface can propagate to another, originally empty, dangling-bond orbital $|b\rangle$, either via (a) the silicon conduction band, or (b) the silicon valence band.

while orbital $|b\rangle$ is empty. If R is large, there will be negligible overlap between the two orbitals, and the only way that the electron in orbital $|a\rangle$ can propagate to orbital $|b\rangle$ is via the silicon valence or conduction bands. There are two possibilities, as illustrated in Fig. 20: (a) the electron in orbital $|a\rangle$ can be virtually excited to the silicon conduction band where it can propagate to the orbital $|b\rangle$ and recombine with the hole in orbital $|b\rangle$, and (b) an electron in the silicon valence band can jump virtually to the orbital $|b\rangle$ and the created hole in the valence band can propagate to the orbital $|a\rangle$ where it recombines with the electron in orbital $|a\rangle$.

The amplitude for the electron to propagate $|a\rangle\rightarrow|b\rangle$ via process (a) can be estimated as follows: Consider the propagator

$$G(a\rightarrow b)=\left\langle b\left|\frac{1}{\omega-H}\right|a\right\rangle . \tag{E1}$$

Let us write $H=H_0+U$, where U is an interaction potential which allows the electron in orbital $|a\rangle$ (or $|b\rangle$) to jump to the conduction state $|\vec{k},c\rangle$. We have

$$\frac{1}{\omega-H_0-U}=G_0+G_0UG_0+G_0UG_0UG_0+\cdots , \tag{E2}$$

where $G_0=(\omega-H_0)^{-1}$. Substituting (E2) into (E1) gives

$$G(a\rightarrow b)=\frac{\mu}{(\omega-E_0)^2-\mu^2} , \tag{E3}$$

where

$$\mu=\sum_k \frac{|\langle \vec{k},c\,|\,U\,|\,a\rangle|^2 e^{i\vec{k}_{||}\cdot\vec{x}_{||}}}{\omega-E_0-V-\hbar^2k^2/2m_c^*}$$

$$\approx-\sum_k \frac{|\langle \vec{k},c\,|\,U\,|\,a\rangle|^2 e^{i\vec{k}_{||}\cdot\vec{x}_{||}}}{V+\hbar^2k^2/2m_c^*} .$$

Here, $H_0\,|\,a\rangle=E_0\,|\,a\rangle$, $\vec{x}_{||}=\vec{x}_b-\vec{x}_a$, is the separation between orbitals $|\,b\rangle$ and $|\,a\rangle$, and m_c^* is the effective mass for an electron near the bottom of the silicon conduction band. For large separation $R=|\,\vec{x}_{||}\,|$, μ can be calculated by asymptotic expansion:[26]

$$\mu\sim R^{-2}\exp[-R(2m_c^*V/\hbar^2)^{1/2}] . \tag{E4}$$

Now, assume that we have a square lattice (lattice constant a) of localized orbitals. The Hamiltonian for this system is written as

$$H=\sum_{i,\delta} t(c_{i+\delta}^{\dagger}c_i+\text{H.c.}) . \tag{E5}$$

Using this Hamiltonian we can again calculate the propagator $G(a\to b)$,

$$G(a\to b)=\frac{t}{(\omega-E_0)^2-t^2} ,$$

and comparing this with (E3) gives $t=\mu$. The energy levels of (E5) are

$$\epsilon_k=4t\sin^2 ka/2\sim tk^2a^2 \quad \text{as } k\to 0 .$$

Thus $m^*\propto 1/(ta^2)$, and with (E4) (note $R=a$),

$$m^*\propto\exp(2m_c^*V/\hbar^2R)^{1/2} ,$$

or

$$m^*(R)=m^*(R_0)\exp[(2m_c^*V/\hbar^2)^{1/2}(R-R_0)] .$$

With $m_c^*=0.18m_e$, $V=0.5$ eV, and measuring R in angstroms, we obtain

$$m^*(R)=m^*(R_0)e^{0.16(R-R_0)} . \tag{E6}$$

From the calculations in Ref. 12 one obtains $|\,m^*(R_0)\,|\simeq 1.5m_e$ when $R_0\simeq 3.85$ Å. Assuming that R_0 is sufficiently large for expression (E6) to be valid, one obtains, for $R=7R_0$, $|\,m^*(R)\,|\simeq 60m_e$. A similar effective mass would be obtained for propagation via the silicon valence band.

[1] A. A. Lucas and M. Šunjić, Phys. Rev. Lett. **26**, 229 (1971); A. A. Lucas and M. Šunjić, Prog. Surf. Sci. **2**, 2 (1972); H. Ibach and D. L. Mills, *Electron Energy Loss Spectroscopy and Surface Vibrations* (Academic, New York, 1982); D. L. Mills, Surf. Sci. **48**, 59 (1975); E. Evans and D. L. Mills, Phys. Rev. B **5**, 4126 (1972); D. M. Newns, Phys. Lett. **60A**, 461 (1979); F. Delanaye, A. Lucas, and G. D. Mahan, Surf. Sci. **70**, 629 (1978); B. N. J. Persson, Solid State Commun. **24**, 573 (1977); D. Šokčević, Z. Lenac, R. Brako, and M. Šunjić, Z. Phys. B **28**, 677 (1977); B. N. J. Persson, Surf. Sci. **92**, 265 (1980); W. L. Schaich, Phys. Rev. B **24**, 686 (1981); W. L. Schaich, Surf. Sci. **122**, 175 (1982).

[2] R. E. Schlier and H. E. Farnsworth, J. Chem. Phys. **30**, 917 (1959); J. J. Lander, in *Progress in Solid State Chemistry*, edited by H. Reiss (Pergamon, Oxford, 1965), Vol. 2, p. 26; W. Mönch, Surf. Sci. **86**, 672 (1979); D. E. Eastman, J. Vac. Sci. Technol. **17**, 492 (1980); D. J. Chadi, Surf. Sci. **99**, 1 (1980); Y. J. Chabal, Phys. Rev. Lett. **50**, 1850 (1983).

[3] See, e.g., F. J. Himpsel, D. E. Eastman, P. Heimann, B. Reihl, C. W. White, and D. M. Zehner, Phys. Rev. B **24**, 1120 (1981).

[4] See, e.g., E. Tosatti and P. W. Anderson, Solid State Commun. **14**, 773 (1974).

[5] U. Backes and H. Ibach, Solid State Commun. **40**, 574 (1981).

[6] U. Backes and H. Ibach, Solid State Commun. **48**, 445 (1983).

[7] L. H. Dubois, G. P. Schwartz, R. E. Camley, and D. L. Mills, Phys. Rev. B **29**, 3208 (1984).

[8] A. A. Lucas and M. Šunjić, Prog. Surf. Sci. **2**, 75 (1972).

[9] W. L. Schaich, Surf. Sci. **122**, 175 (1982). G. D. Mahan, *Many Particle Physics* (Plenum, New York, 1981), p. 223.

[10] D. L. Mills, Surf. Sci. **48**, 69 (1975).

[11] F. J. Himpsel, D. E. Eastman, P. Heimann, B. Reihl, C. W. White, and D. M. Zehner, Phys. Rev. B **24**, 1120 (1981); J. E. Demuth, B. N. J. Persson, and A. J. Schell-Sorokin, Phys. Rev. Lett. **51**, 2214 (1983).

[12] J. A. Appelbaum and D. R. Hamann, Phys. Rev. Lett. **32**, 225 (1974); S. Ciraci, I. P. Batra, and W. A. Tiller, Phys. Rev. B **12**, 5811 (1975); M. Schlüter, J. R. Chelikowsky, S. G. Louie, and M. L. Cohen, *ibid.* **12**, 4200 (1975); K. C. Pandey and J. C. Phillips, *ibid.* **13**, 750 (1976).

[13] W. A. Harrison, Surf. Sci. **55**, 1 (1976).

[14] H. Froitzheim, U. Köhler, and H. Lammering (unpublished).

[15] The dispersion relation for plasmons in two dimensions is determined by the pole of $g(q_{||},\omega)$ [see Eq. (19)]: $\omega^2=4\pi ne^2q_{||}/[m^*(\epsilon+1)]$. Thus there are plasmons with arbitrary small frequency ω.

[16] R. J. Culbertson, L. C. Feldman, and P. J. Silverman, J. Vac. Sci. Technol. **20**, 868 (1982).

[17] Y. J. Chabal, Phys. Rev. Lett. **50**, 1850 (1983); Y. J. Chabal, G. S. Higashi, and S. B. Christman, Phys. Rev. B **28** 4472 (1983).

[18] E. Conrad and M. B. Webb, Surf. Sci. **129**, 37 (1983).

[19] G. Binning, H. Rohrer, Ch. Gerber, and E. Weibel, Phys. Rev. Lett. **50**, 1850 (1983).

[20] C. B. Duke and W. K. Ford, Surf. Sci. **111**, L685 (1981); S. Doniach, Adv. Phys. **18**, 819 (1969).

[21] E. Louis, C. Tejedor, and F. Flores, Solid State Commun. **47**, 939 (1983); E. Louis, F. Flores, F. Guinea, and C. Tejedor, *ibid.* **44**, 633 (1982).

[22] M. Wittner, D. L. Smith, P. W. Lew, and M. A. Nicolet Solid State Electron. **21**, 573 (1978).

[23] G. W. Rubloff, Surf. Sci. **132**, 268 (1983), and references therein.

[24] J. M. Ziman, *Electrons and Phonons* (Oxford University Press, London, 1960), p. 467.

[25] S. Andersson, B. N. J. Persson, M. Persson, and N. D. Lang, Phys. Rev. Lett. **52**, 2073 (1984).

[26] See the Appendix in B. N. J. Persson, Surf. Sci. **116**, 585 (1982).